Chapter 2. Climate Simulations, Land Cover, and Wildfire

By T. Scott Rupp,[1] Paul Duffy,[2] Matthew Leonawicz,[1] Michael Lindgren,[1] Amy Breen,[1] Tom Kurkowski,[1] Angelica Floyd,[1] Alec Bennett,[1] and Lena Krutikov[1]

2.1. Highlights

- Climate models suggest a projected annual and seasonal increase in mean temperature throughout Alaska during the next 85 years. Warming has been projected to be greatest in the winter and spring and most pronounced in the northern and western regions of the State.
- Winter temperatures are projected to increase by as much as 8 degrees Celsius (°C) in the Arctic and Western Alaska Landscape Conservation Cooperatives (LCCs) by the end of this century.
- Wildfires burned an annual average of 3,791 square kilometers (km^2) between 1950 and 2009 in Alaska. The inter-annual variability in the area that was burned was high—from as few as 10 km^2 burned in 1961, 1964, and 1965 to as much as 27,071 km^2 burned in 2004.
- Wildfire frequency and extent are projected to increase across most of the six future climate simulations used in this assessment and across the five LCC regions, with the Northwest Boreal LCC North projected to see the largest increase in fire activity.
- The areas of late successional boreal forest land cover are projected to decrease under almost all climate simulations, ranging from approximately 8 to 44 percent; a concomitant increase in early successional deciduous forest land cover is also projected.
- Under most of the future climate simulations used in this assessment, the area of graminoid tundra land cover is projected to decrease whereas the area of shrub tundra land cover is projected to increase.

2.2. Introduction

As indicated in chapter 1, the ongoing warming trend of northern high-latitude regions, which influences vegetation distribution, ecosystem disturbances, and their interactions, has the potential to substantially alter the overall ecosystem carbon balance. Development of baseline and projected land-cover and wildfire data as well as the driving climate projections provide several of the primary spatial data foundations for this assessment. The simulations of future land-cover change and wildfire activity feed into other components of the assessment—primarily the simulation of carbon storage and greenhouse-gas (GHG) fluxes (see chapters 6 and 7).

Global temperature increases during the 20th century (Solomon and others, 2007) were amplified at high latitudes (Chapman and Walsh, 1993; Serreze and others, 2000; Overland and others, 2004; Serreze and Francis, 2006). In Alaska, warming since the 1950s appears to be unprecedented in at least the past 400 years (Overpeck and others, 1997; Barber and others, 2004; Kaufman and others, 2009). Mean annual air temperature in the boreal region of interior Alaska has increased by 1.3 degrees Celsius (°C) during the past 50 years, with the greatest warming occurring in winter (Hartmann and Wendler, 2005; Shulski and Wendler, 2007). Air temperature is projected to increase by an additional 3 to 7 °C by the end of this century (Walsh and others, 2008).

Across Alaska, significant shifts in vegetation composition and production have been observed, including yellow-cedar (*Callitropsis nootkatensis* (D. Don) D.P. Little) decline throughout the coastal temperate forest region (Hennon and others, 2006), decreased spruce growth in boreal Alaska (Barber and others, 2000; McGuire and others, 2010; Beck and others, 2011), woody vegetation encroachment into wetlands (Berg and others, 2009), and positive productivity throughout tundra regions with concurrent negative productivity throughout forested regions (for example, Goetz and

[1]University of Alaska-Fairbanks, Fairbanks, Alaska.

[2]Neptune and Company, Inc., Fort Collins, Colo.

others, 2005; Verbyla, 2008; Beck and others, 2011). Recent changes in major disturbance regimes in Alaska are linked to changes in climate. Wildfire, the dominant driver of ecosystem change in much of Alaska, is strongly linked to climate, where the average June temperature explains 78 percent of the inter-annual variability in total area burned (Duffy and others, 2005). In the past decade, the average annual area burned has doubled compared with any decade of the previous 50 years (Kasischke and others, 2010).

This chapter describes the methodology and results for the foundational modeling work required for this assessment. The following sections describe the major input datasets used for the entire assessment process, including climate, land cover, and wildfire; a description of the transient biogeographic model Alaska Frame-Based Ecosystem Code (ALFRESCO) and the methodology used for the simulation and analysis of climate-vegetation-wildfire dynamics follows. The result sections first present the historical period (1950–2009), followed by the projection period (2010–2099). Both the historical and projected periods sections contain specific subsections covering climate, vegetation, and wildfire trends.

2.2.1. Climate

Alaska's large climate gradient is influenced by latitude, elevation, and proximity to water bodies, including the influence of sea ice. This is reflected in the distribution of maritime, transitional, and continental climates across the State.

The most recent U.S. National Climate Assessment—Alaska Technical Regional Report (Markon and others, 2012), which included a comprehensive synthesis of the literature on Alaska's climate records, indicated that average annual statewide temperatures have increased significantly—on the order of 2 °C over the past 50 years (Stafford and others, 2000; Shulski and Wendler, 2007). The warming is not uniform across the State and is not consistent across seasons. The greatest observed temperature increases have occurred over winter and spring—at two to three times the level of warming found in summer and fall. Regionally, the interior continental portions of the State have experienced the most warming, with some areas experiencing an increase of more than 4 °C, whereas coastal and maritime areas have experienced change on the order of 0.5 to 1 °C (Shulski and Wendler, 2007).

A significant portion of the observed warming in Alaska occurred as a sudden, step-like change in the mid-1970s coinciding with a major shift in the Pacific Decadal Oscillation (PDO) (Markon and others, 2012). The PDO index captures this shift as a transition from predominantly negative to predominantly positive values around 1976–77 (Mantua and others, 1997). The temperature increase in Alaska, however, mirrors trends across the arctic and subarctic (Hinzman and others, 2005; Solomon and others, 2007), suggesting that large-scale atmospheric circulation patterns (such as PDO) may have amplified or accelerated an underlying long-term warming trend.

These climate dynamics further highlighted the need to identify the most accurate general circulation models (GCMs) to develop realistic and consistent climate simulations to be used in this assessment. Walsh and others (2008) evaluated the Coupled Model Intercomparison Project phase 3 (CMIP3; Meehl and others, 2007) models to identify the best performing GCMs for the Alaska region. The core statistic of the study was a root-mean-square-error (RMSE) evaluation of the differences between mean model output for each grid point and calendar month, and data from the European Centre for Medium-Range Weather Forecasts (ECMWF) Reanalysis, ERA–40. ERA–40 is one of the most consistent and accurate gridded representations of these variables available. From this analysis, the best performing CMIP3 models were identified for further consideration.

The climate data described here were aligned with the Intergovernmental Panel on Climate Change's Special Report on Emissions Scenarios (IPCC-SRES; Nakićenović and Swart, 2000). This assessment used three emissions scenarios (A2, A1B, and B1, from high to low projected carbon dioxide emissions; table 2.1) to force the GCMs and capture the uncertainties within and across the models. Two of the best performing CMIP3 models were used in this assessment—version 3.1-T47 of the Canadian Centre for Climate Modelling and Analysis' Coupled Global Climate Model (CGCM3.1; McFarlane and others, 1992; Flato, 2005) and version 5 of the Max Planck Institute's European Centre Hamburg Model (ECHAM5; Roeckner and others, 2003, 2004). The selected GCMs represented a range of projected climate change and were those to which the fire regime simulations were considered sensitive.

2.2.2. Land Cover

Land cover in Alaska includes substantial expanses of forest (both boreal and maritime) and tundra (including shrub-dominated and heath). There are six level II ecoregions covered by this assessment (see chapter 1). These six ecoregions correspond approximately to four primary Landscape Conservation Cooperatives (LCCs) in Alaska, which were used to summarize regional ecosystem characteristics.

Unlike the rest of the United States, Alaska does not have a consistent high-spatial-resolution remote sensing product that provides regular land-cover classification statewide, nor does it have consistent and widespread vegetation monitoring networks across the State. To simulate biological processes, including plant growth dynamics, tree line dynamics, vegetation composition and distribution, wildfire, and biogeochemistry across the landscape, this assessment used the North American Land Change Monitoring System (NALCMS) 2005 dataset (North American Land Change Monitoring System, 2010; for arctic and subarctic ecosystem types) and the National Land Cover Database (NLCD) 2001 (Homer and others, 2007; for coastal temperate forest ecosystem types). See chapter 1 for descriptions of the input land-cover data.

Table 2.1. Assumptions about the primary driving forces affecting land-use and land-cover change.

[These assumptions were used to downscale the B1, A1B, and A2 and scenarios, in order of low to high projected CO_2 emissions, of the Intergovernmental Panel for Climate Change's Special Report on Emissions Scenarios (Nakićenović and Swart, 2000). Population and per capita income projections are from Strengers and others (2004)]

Driving forces	A1B	A2	B1
Population growth (global and United States)	Medium; globally, 8.7 billion by 2050, then declining; in the United States, 385 million by 2050	High; globally, 15.1 billion by 2100; in the United States, 417 million by 2050	Medium; globally, 8.7 billion by 2050, then declining; in the United States, 385 million by 2050
Economic growth	Very high; U.S. per capita income $72,531 by 2050	Medium; U.S. per capita income $47,766 by 2050	High; U.S. per capita income $59,880 by 2050
Regional or global innovation	Global	Regional	Global
Technological innovation	Rapid	Slow	Rapid
Energy sector	Balanced use	Adaptation to local resources	Smooth transition to renewable
Environmental protection	Active management	Local and regional focus	Protection of biodiversity

2.2.3. Wildfire

Climate warming is also thought to be responsible for recent changes in fire regime in North American high-latitude regions (Gillett and others, 2004). In recent decades, annual area burned has increased in Alaska (Kasischke and Turetsky, 2006; Kasischke and others, 2010) and Canada (Gillett and others, 2004) and is hypothesized to have increased in Eurasia (Hayes and others, 2011; Kharuk and others, 2013). Several studies indicate that this increase would be maintained at least during the first half of the 21st century (Balshi and others, 2009; Mann and others, 2012). Greater burned area as well as possible changes in fire severity have substantial implications for permafrost, as increased severity leads to greater consumption of the organic layer that may increase active-layer thickness (Dyrness and Norum, 1983; Yoshikawa and others, 2002; Burn and others, 2009; Genet and others, 2013) and may potentially cause thermokarst disturbance in ice-rich soils (Jorgenson and others, 2001; Myers-Smith and others, 2008). Carbon cycling, albedo, and stand structure in the boreal forest are strongly influenced by the frequency and severity of wildfires (Randerson and others, 2006; Euskirchen and others, 2009; Johnstone and others, 2010; Turetsky and others, 2011), and burning is an important disturbance mechanism by which stored carbon is released to the atmosphere (Kasischke and others, 2000, 2005; Amiro and others, 2001).

A synthesis of contemporary fire trends in Alaska by Kasischke and others (2010) suggests a mixture of climatic and human controls on fire patterns. Between 2000 and 2009, an annual average of 7,670 square kilometers (km^2) was burned, 50 percent more area burned than in any previous decade since the 1940s. Over the past 60 years, there was a decrease in the number of lightning-ignited fires, an increase in extreme lightning-ignited fire events, an increase in human-ignited fires, and a decrease in the number of extreme human-ignited fire events. The fraction of area burned from human-ignited fires fell from 26 percent for the 1950s and 1960s to 5 percent for the 1990s and 2000s as a consequence of the change in fire policy that gave the highest suppression priorities to fire events that occurred near human settlements. The amount of area burned during late-season fires has also increased over the past two decades. Deeper burning of surface organic layers in black spruce (*Picea mariana* (Mill.) Britton, Sterns & Poggenb.) forests occurred during late-growing-season fires and on more well-drained sites, with consequences for forest regeneration. These trends all point to the importance of accounting for the potential changes in the Alaska fire regime with respect to a credible assessment of carbon storage and fluxes.

2.2.4. Other Drivers of Land-Cover Change

As discussed in the preceding sections, land-cover changes in Alaska are driven primarily by climate-induced environmental variability and disturbance (primarily wildfire-associated forest mortality and succession). There are, however, other drivers of land-cover change acting upon specific portions of the Alaskan landscape. For example, insects are affecting forests in the southern portions of the Alaskan boreal forest. In recent decades, warmer temperatures contributed to spruce beetle outbreaks, in part owing to a reduction of the beetle life cycle from 2 years to 1 year (Werner and others, 2006). This reduction in life cycle of an endemic species allowed populations to exceed critical thresholds that ultimately led to mortality across all forest age classes. This has led to white spruce (*Picea glauca* (Moench) Voss) mortality throughout the region of 12,000 km^2 between 1990 and 2000 (Werner and others, 2006). In addition, earlier snowmelt and persistent early spring freezing have had important implications for Alaska cedar decline in the coastal temperate forest region of Alaska, where over 2,000 km^2 of pristine forests have died in the past 100 years (Hennon and others, 2006). The loss of thermal cover and associated

dehardening of the species in late winter has resulted in fine-root damage in early spring.

Agricultural lands in Alaska occupy a small portion of the total land area of the State. Although roughly 90,000 km^2 have been identified as having current agricultural potential, only 0.1 percent is currently being cropped (U.S. Department of Agriculture, National Agricultural Statistics Service, 2014). Likewise, human settlements contribute a minor fraction of the Alaskan land cover. State population is approximately 736,000, which equates to approximately 2 persons per square kilometer. Although these other land-cover-change drivers impart little influence on the overall carbon assessment of Alaska, these drivers could play a larger role in altering the future carbon budget—especially with respect to forest insect- and disease-related mortality.

2.3. Input Data and Methods

2.3.1. Input Data Sources

The PRISM (Parameter-elevation Relationships on Independent Slopes Model; http://www.prism.oregonstate.edu) by Daly and others (2008) was used to provide gridded climate normals (monthly temperature and precipitation) for 1961–1990 at a 2-kilometer (km) spatial resolution. These data were resampled to 1 km and used as the baseline climatology for the climate downscaling procedure.

We used the CRU TS v. 3.10.01 high-resolution (0.5 degree [°]×0.5°) gridded data (Harris and others, 2014) from the Climatic Research Unit (CRU; http://www.cru.uea.ac.uk) at the University of East Anglia to provide historical climate data for the period 1950–2009. These data were downscaled and served as driving climate data input for the retrospective model simulations including model spin-up, which used the downscaled CRU data starting in 1900.

Analysis and synthesis of historical fire activity data (1950–2009) were based on estimates from fire management records maintained by the Alaska Interagency Coordination Center (M. Henderson, Alaska Interagency Coordination Center, unpub. data, June 1, 2010). This database includes digitized fire perimeters, which were used to generate summary statistics across the assessment domain as well as the five LCC regions and for both annual and decadal time periods. The tables and figures presented in the historical fire activity subsection summarize these results.

2.3.2. Methods and Analysis

The baseline period for this assessment was defined as the period from 1950 through 2009. This historical period is bounded by the beginning of reliable wildfire observations and statistics (1950) and the end of contemporary downscaled historical climate observations (2009). The projection period was defined as the period from 2010 through 2099. The results in this chapter, both historical and projected, were summarized across the full assessment domain as well as for the five LCC regions described in chapter 1.

Historical (CRU TS v. 3.10.01) and projected (CMIP3) output variables of surface temperature and precipitation were downscaled via the delta method (Hay and others, 2000; Hayhoe, 2010) using PRISM 1961–1990 2-km-resolution climate normals as baseline climate (Daly and others, 2008). The delta method was implemented by calculating climate anomalies applied as differences for temperature or quotients for precipitation between monthly future CMIP3 data and calculated CRU climate normals for 1961–1990 (see http://www.snap.uaf.edu for data and details). These coarse-resolution anomalies were then interpolated to PRISM spatial resolution via a spline technique and then added to (temperature) or multiplied by (precipitation) the PRISM climate normals. The downscaled climate data were then interpolated to a 1-km resolution for modeling purposes. Our modeling used the two GCMs of the best performing subset models for Alaska (Walsh and others, 2008), which bound the climate scenarios from most warming (ECHAM5) to least warming (CGCM3.1). Each model was downscaled for the three emissions scenarios (A1B, A2, B1; table 2.1).

Historical (CRU) and projected (CMIP3) output variables of surface downwelling shortwave radiation (RSDS; expressed as megajoules per square meter per day) and vapor pressure (VP; expressed as hectopascals) were calculated and downscaled for use by the biogeochemical Terrestrial Ecosystem Model (TEM). The historical data constitute the result of the delta-method downscaling procedure using the monthly time series (CRU TS v. 3.10.01; 1950–2009, 0.5° spatial resolution) and global climatology (CRU CL v. 2.0; 1961–1990, 10-minute spatial resolution) data. The projected data constitute the same CMIP3 models used for temperature and precipitation. The data were bias corrected and downscaled to 1-km resolution.

For the surface downwelling shortwave radiation data, the baseline climatology for the top of the atmosphere solar radiation data (referred to as *girr*) was calculated using an equation from Allen and others (1998) at a monthly timestep, which is used to represent the historical period RSDS data at 1-km spatial scale. The downscaled cloud cover time series was then used to calculate the surface solar radiation (referred to as *nirr*) from *girr* and downscaled cloud cover using the following equation:

$$nirr = monthly\_girr \times (0.251 + (0.509(1.0 - cloud\_cover/100))) \quad (2.1)$$

The CRU TS v. 3.10.01 data are distributed as vapor pressure and were converted to relative humidity using the conversion equation from the World Meteorological Organization's Commission for Instruments and Methods of Observation (CIMO) guide (2008) using the following equations:

$$saturated\_vapor\_pressure = 6.112 \times \exp((22.46 \times temperature)/(272.62 + temperature)) \quad (2.2)$$

$$relative\_humidity = (vapor\_pressure / saturated\_vapor\_pressure) \times 100 \quad (2.3)$$

Proportional anomalies were then generated using the newly converted CRU TS v. 3.10.01 historical VP data where the climatological period used was 1961–1990. These CRU TS v. 3.10.01 proportional anomalies were then interpolated using a spline interpolation to a 10-minute resolution grid for downscaling with the CRU CL v. 2.0 relative humidity data. The final step was to convert the downscaled relative humidity data to vapor pressure using the below conversion equation:

$$saturated\_vapor\_pressure = 6.112 \times \exp((17.62 \times temperature)/(243.12 + temperature)) \quad (2.4)$$

$$vapor\_pressure = (relative\_humidity \times saturated\_vapor\_pressure)/100 \quad (2.5)$$

Additional methodological details for all the downscaled climate variables can be found in the individual metadata files at the Scenarios Network for Alaska and Arctic Planning (SNAP) data download Web site (https://www.snap.uaf.edu/tools/data-downloads).

We used the biogeographic simulation model ALFRESCO (Rupp and others, 2000, 2002, 2007; Johnstone and others, 2011; Mann and others, 2012; Gustine and others, 2014; Amy Breen, University of Alaska-Fairbanks, written commun., January 15, 2015) to simulate changes in vegetation dynamics and fire regime for the projection period (2010–2099) in response to the climate simulations used in this assessment. ALFRESCO is a spatially explicit, stochastic landscape succession model for arctic, subarctic, and boreal vegetation types that operates in the Alaska and Northwest Canada region at a 1-km resolution and an annual timestep. The model represents seven general vegetation types (shrub tundra, graminoid tundra, wetland tundra, white spruce forest, black spruce forest, early successional deciduous forest, and coastal temperate forest) in Alaska. Currently, the coastal temperate forest and the wetland tundra vegetation types are represented as static vegetation states.

The fire module of ALFRESCO uses a cellular automata approach with separate subroutines for cell ignition and spread to simulate annual fire season activity. Both ignition and fire spread (that is, flammability) are a function of growing-season climate (Duffy and others, 2005), vegetation type, and time since last fire. The ignition of any given cell is stochastic in nature and determined by comparing a randomly generated number against the flammability coefficient of that cell. The flammability coefficient allows for changes in flammability that take place through succession (that is, fuel build up).

Following a wildfire in ALFRESCO, general successional trajectories for forested systems are as follows: burned spruce forest (white or black) transitions into early successional deciduous forest, and burned deciduous forest self-replaces. Vegetation transition times differed probabilistically between climax black and white spruce trajectories (Rupp and others, 2002). Transitional times were modeled probabilistically to represent early successional (that is, recolonization) deciduous forest following wildfires in spruce and deciduous forest and to determine the amount of time, in the absence of fire, until the climax spruce stage dominates the site again. Self-replacement of deciduous forest can occur when repeated burning and (or) climate conditions preclude transition to climax spruce. ALFRESCO incorporates the effects of fire severity on transition times using measurements of the area of the wildfire (that is, fire size), complex topography, and vegetation type on flat landscapes (Duffy and others, 2007; Johnstone and others, 2011).

Transitions in tundra are driven by succession or colonization and infilling. These processes are influenced by climate and fire history, which affect seedling establishment and growth conditions and proximity to seed source (Breen and others, written communication). For the transition from tundra to forest at the tree line, seed dispersal occurs within a 1-km neighborhood. White spruce colonization and infilling are possible in both graminoid and shrub tundra with transition rates to spruce forest mediated by climate effects and basal area growth. Vegetation succession from graminoid to shrub tundra is modeled probabilistically, with a greater likelihood of transition to shrub tundra post-fire. In the case of wildfire activity, shrub tundra transitions to graminoid tundra and graminoid tundra self-replaces. Wetland tundra in the model does not currently burn and is represented as a static vegetation type.

The relationship between climate and fire was calibrated by comparing model output (such as, fire regime, stand age structure) to the corresponding historical data (Mann and others, 2012). Simulated vegetation and fire dynamics were analyzed and synthesized across the full ensemble of simulations (number of replicates [n]=200) and for all six climate simulations (combinations of the three emissions scenarios and the two GCMs) used in this assessment. Vegetation transitions, defined as at least one shift in vegetation type during the projection period (2010–2099), were calculated as a percent of total area for each of the five LCC regions. Tables and figures presented in the projected land-cover and wildfire subsections include synthesis of these results.

2.4. Results and Discussion

2.4.1. Baseline Land Cover

Our baseline land-cover classes for the assessment domain, based on the NALCMS remote sensing product from 2005, consisted of forest (51 percent), tundra (28 percent), and nonvegetated (21 percent) (table 2.2). Forest land cover was dominated by early successional deciduous forest (30 percent), followed by white spruce forest (9 percent), black spruce forest (6 percent), and coastal temperate forest (6 percent). Tundra land cover was dominated by shrub tundra (17 percent), followed by graminoid tundra (10 percent) and wetland tundra (1 percent). The nonvegetated regions were composed of rock, ice, snow, water, and coastlines and represent land-cover classes not modeled.

Table 2.2. Land-cover types used in this assessment for the Alaska Frame-Based Ecosystem Code (ALFRESCO) model simulations, percent of area, and the source of the input data.

[Percent of area calculated in 2005. Land-cover types ordered from late to early successional forest to tundra to other cover types. NALCMS 2005, North American Land Change Monitoring System 2005 dataset; NLCD 2001, 2001 National Land Cover Database]

Land-cover type	Area (percent)	Source
Black spruce forest	6	NALCMS 2005
White spruce forest	9	NALCMS 2005
Deciduous forest	30	NALCMS 2005
Shrub tundra	17	NALCMS 2005
Graminoid tundra	10	NALCMS 2005
Wetland tundra	1	NALCMS 2005
Heath tundra	0	NALCMS 2005
Coastal temperate forest	6	NLCD 2001
Nonvegetated	21	NALCMS 2005

The Arctic LCC is dominated by tundra land-cover types with a relatively even distribution between shrub and graminoid tundra, 108,226 square km^2 and 119,027 km^2, respectively (table 2.3). There were minor components of deciduous forest (15,460 km^2) and wetland tundra (10,621 km^2) and very small components of black and white spruce forests.

The Western Alaska LCC has a relatively even distribution of tundra land-cover types and deciduous forest (table 2.3). Deciduous forest (130,904 km^2) is the dominant land-cover type. The LCC also has minor components of white and black spruce forests (9,424 km^2 and 5,873 km^2, respectively). Of the tundra land-cover types, shrub tundra dominates (119,517 km^2) with a minor component of graminoid tundra (12,379 km^2) and a very small component of wetland tundra. There is also a minor component of coastal temperate forest (9,268 km^2) within the LCC and along the border with the far northwestern portion of the North Pacific LCC.

The Northwest Boreal LCC North and South are both dominated by boreal forest land-cover types (table 2.3). In the Northwest Boreal LCC South, early successional deciduous forest dominates (66,673 km^2), followed by white spruce (18,706 km^2) and then black spruce (11,812 km^2). In the Northwest Boreal LCC North, there is a similar distribution of forest land-cover types; however, the areal extent is significantly greater than the Northwest Boreal LCC South. In the Northwest Boreal LCC North, early successional deciduous forest dominates (238,414 km^2), followed by white spruce (101,688 km^2) and then black spruce (77,183 km^2). Both LCC regions also have minor components of tundra land-cover types; however, neither region contains wetland tundra. The

Table 2.3. Land-cover types used in this assessment summarized by area for the five Landscape Conservation Cooperative (LCC) regions.

[Data may not add to totals shown because of independent rounding. km^2, square kilometer]

LCC region	Area in 2005 (km^2)									
	Black spruce forest	White spruce forest	Deciduous forest	Shrub tundra	Graminoid tundra	Wetland tundra	Heath tundra	Coastal temperate forest	Non-vegetated	Total
Arctic LCC	248	648	15,460	108,226	119,027	10,621	0	0	54,363	**308,593**
Western Alaska LCC	5,873	9,424	130,904	119,517	12,379	515	0	9,268	90,341	**378,221**
Northwest Boreal LCC North	77,183	101,688	238,414	11,942	16,961	0	9	0	10,387	**456,584**
Northwest Boreal LCC South	11,812	18,706	66,673	12,961	3,238	0	0	2,542	70,371	**186,303**
North Pacific LCC	636	392	603	8	2	0	0	75,999	85,721	**163,361**

Northwest Boreal LCC South contains a minor component of coastal temperate forest along the southern boundary and along the border with the North Pacific LCC.

The North Pacific LCC is dominated by coastal temperate forest (75,999 km^2) as well as nonvegetated areas, mostly snow and ice (table 2.3). There are very small components of boreal forest land-cover types in the extreme northern portion of the LCC bordering the Northwest Boreal LCC South.

2.4.2. Baseline Wildfire

From fire management records, the number of wildfires between 1950 and 2009 across the full simulation domain of this assessment ranged from as high as 176 fires in 2005 to less than or equal to 1 in 1952, 1961, 1964, and 1965 (table 2.4). The minimum number of fires is difficult to estimate owing to detection issues associated with the remoteness and size of Alaska. These issues were likely more pronounced in the earlier period of the historical data. Consequently, the estimate of the minimum number of fires is highly uncertain. Similar issues exist with the estimation of area burned in years with little activity. Annual area burned averaged 3,791 km^2—that is, 0.25 percent of the total area of the Alaska simulation domain, which has a total area of 1.49 million km^2. The maximum annual area burned was 27,071 km^2 (that is, 1.3 percent of the total area), which occurred in 2004. There were three years (1961, 1964, and 1965) where less than 10 km^2 were recorded as being burned. As reported by Kasischke and others (2002), the wildfire perimeter records for the 1960s were rated fair and included many missing data records. Historical data for each of the LCC regions is subsequently discussed in order of decreasing fire activity as measured by annual area burned.

The Northwest Boreal LCC North had most (approximately 85 percent of the statewide total) of the fire activity among the five LCC regions of the assessment (table 2.4, fig. 2.1). The number of wildfires between 1950 and 2009 ranged from a high of 137 in 2005 to 0 in both 1961 and 1964. The annual area burned averaged 3,262 km^2. The inter-annual variability in area burned was high, and area burned ranged from 0 km^2 in both 1961 and 1964 to 26,684 km^2 in 2004. The range of annual area burned was between 0 and 5.8 percent of the Northwest Boreal LCC North, which has a total area of 456,584 km^2.

The Western Alaska LCC had the second most (approximately 10 percent) fire activity among the five LCC regions of the assessment (table 2.4, fig. 2.1). In the Western Alaska LCC, the number of wildfires between 1950 and 2009 averaged 6 per year—with a high of 37 in 1972 and 13 years recording no fires. Annual area burned averaged 394 km^2, or 0.1 percent of the Western Alaska LCC, which has a total area of 378,221 km^2. The range of annual area burned was between 0 and 2.2 percent of the Western Alaska LCC.

In the Arctic LCC, the number of wildfires between 1950 and 2009 averaged 2 per year—with a high of 13 in 2005 and 31 years recording no fires (table 2.4, fig. 2.1). Annual area

Table 2.4. Baseline (1950–2009) wildfire statistics for each Landscape Conservation Cooperative (LCC) region and the full assessment domain (Alaska).

[Data from fire management records maintained by the Alaska Interagency Coordination Center. km^2, square kilometer]

Metric	Number of wildfires per year	Annual area burned (km^2)
Arctic LCC		
Mean	2.1	60.49
Standard deviation	3.2	178.16
Minimum	0	0
Median	0	0
Maximum	13	1,106.82
Year of maximum	2005	2007
Western Alaska LCC		
Mean	5.82	393.81
Standard deviation	7.68	1,258.46
Minimum	0	0
Median	3.5	33.42
Maximum	37	8,313.5
Year of maximum	1972	1957
Northwest Boreal LCC North		
Mean	31.8	3,262.26
Standard deviation	33.07	5,178.67
Minimum	0	0
Median	20	1,296.82
Maximum	137	26,683.54
Year of maximum	2005	2004
Northwest Boreal LCC South		
Mean	2.15	54.49
Standard deviation	2.7	112.52
Minimum	0	0
Median	1	4.28
Maximum	15	615.4
Year of maximum	2009	2009
North Pacific LCC		
Mean	0.6	2.21
Standard deviation	0.92	6.93
Minimum	0	0
Median	0	0
Maximum	4	36.31
Year of maximum	1991	1991
Alaska		
Mean	41.3	3,791.5
Standard deviation	41.92	5,709.97
Minimum	0	0
Median	27	1,596.77
Maximum	176	27,071.72
Year of maximum	2005	2004

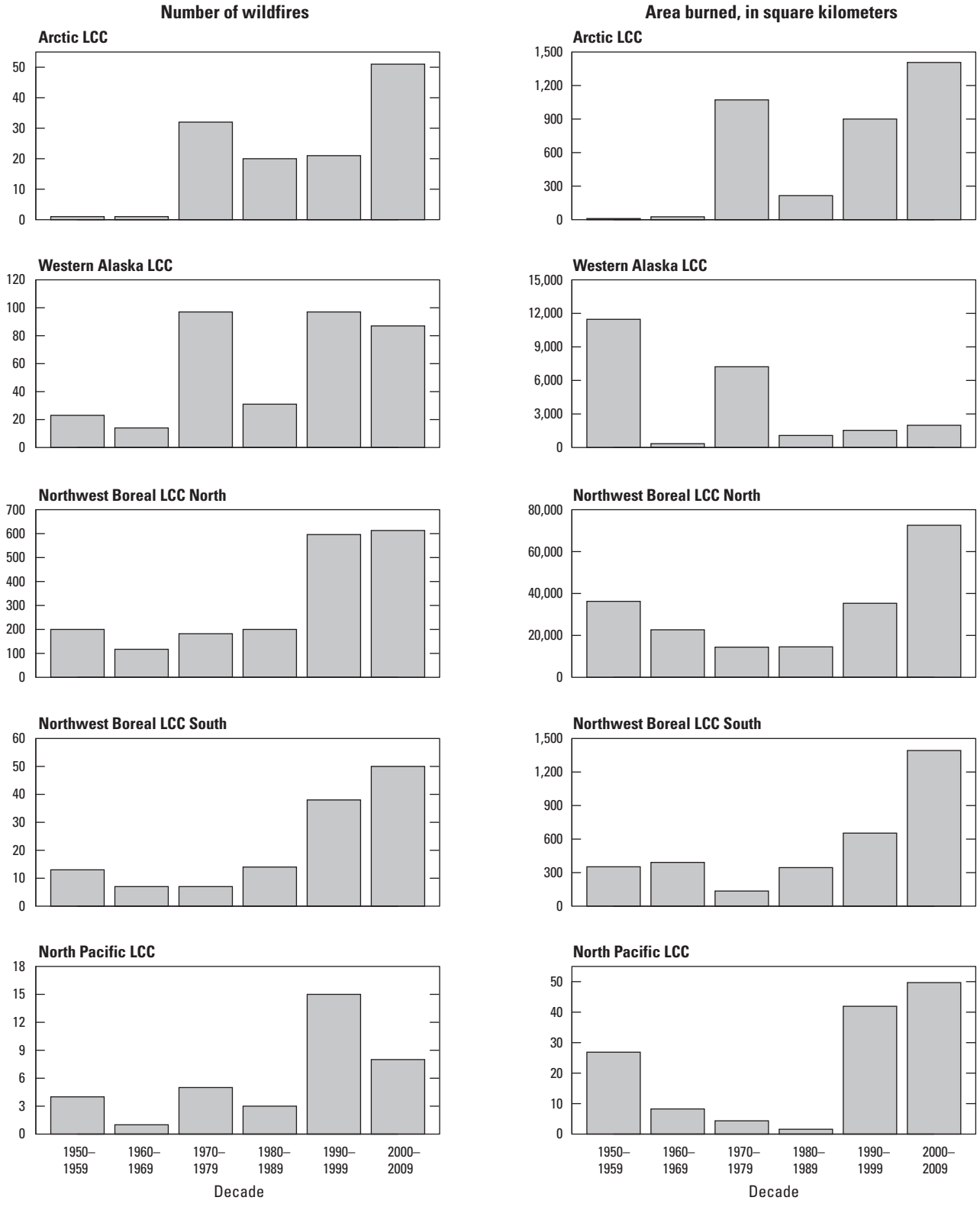

Figure 2.1. A decadal summary of number of wildfires and area burned for each Landscape Conservation Cooperative (LCC) region for the historical period (1950–2009).

burned averaged 60 km², or 0.01 percent of the Arctic LCC, which has a total area of 308,593 km². The range of annual area burned was between 0 and 0.35 percent of the Arctic LCC.

In the Northwest Boreal LCC South, the number of wildfires between 1950 and 2009 averaged 2 per year—with a high of 15 in 2009 and 15 years recording no fires (table 2.4, fig. 2.1). Annual area burned averaged 54 km², or 0.03 percent of the Northwest Boreal LCC South, which has a total area of 186,303 km². The range of annual area burned was between 0 and 0.33 percent of the Northwest Boreal LCC South.

Of the five assessment regions, the North Pacific LCC had the least amount of fire activity reflecting the LCC's wet and cool climate (table 2.4, fig. 2.1). The number of wildfires between 1950 and 2009 averaged 1 per year—with a high of 4 in 1991 and 37 years recording no fires. Annual area burned averaged 2 km² and ranged from 0 to 36 km². The range of annual area burned was between 0 and 0.02 percent of the North Pacific LCC, which has a total area of 163,361 km².

2.4.3. Climate Simulations

Visualizations of seasonal baseline (1950–2009) climate patterns for mean monthly temperature in degrees Celsius (°C) and total monthly precipitation in millimeters (mm), based on the downscaled CRU data (http://www.snap.uaf.edu), are presented in figure 2.2. The downscaled CRU historical period data exhibited strong variability across seasons and also indicated high spatial variability.

Figure 2.3 and table 2.5 present projected changes in mean monthly temperature (°C) and total precipitation (mm) by season, calculated using the difference in mean values from the last two decades of the historical period (1980–2009) to those of the projection period (2070–2099). Warming trends are projected by both GCMs and across all three emissions scenarios. Warming would be greatest in the northern and western regions of Alaska. There was greater projected variability among the scenarios than between GCMs. The A2 scenario projected the greatest warming and the B1 scenario the least warming. The ECHAM5 climate simulations project warmer temperatures than the CGCM3.1 simulations. Projected warming is not uniform seasonally and both GCMs project substantially greater warming during the winter (December, January, February) and fall (September, October, November). Growing season (defined here as April through September) is a particularly important annual time period as plant production and wildfire activity are constrained within these months. Growing season temperatures are projected to increase in all six climate simulations (fig. 2.4) across the full assessment period (1950–2099).

Precipitation increases are also projected by both GCMs and across all three emissions scenarios (table 2.5). Across the full assessment domain, differences between GCMs were

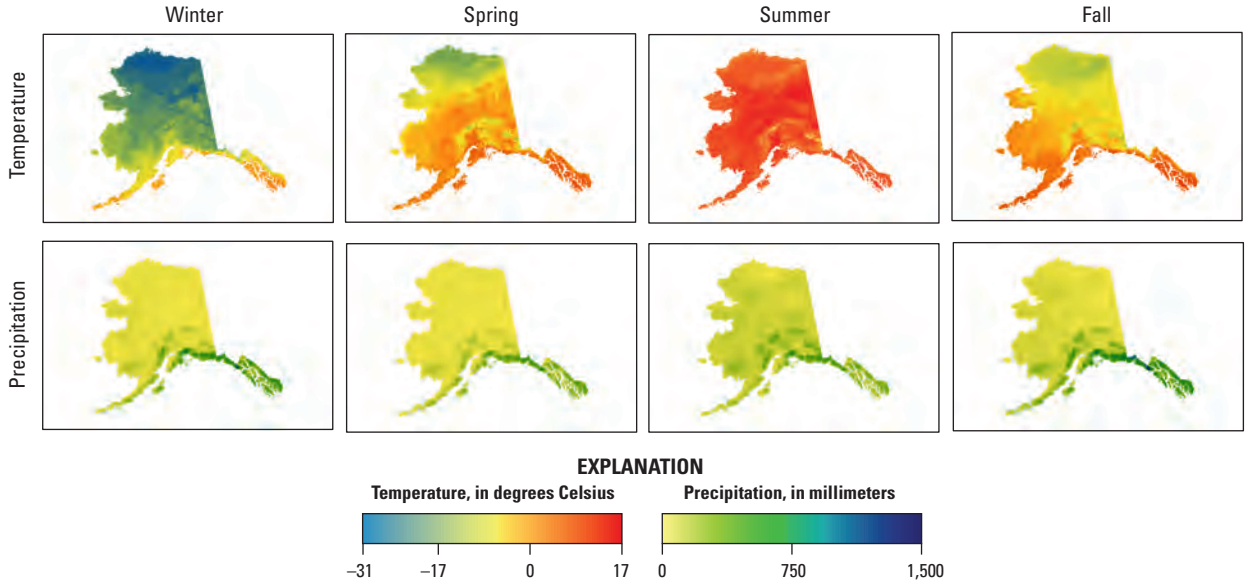

Figure 2.2. Baseline (1950–2009) seasonal mean monthly temperature and total precipitation by season using downscaled Climate Research Unit data (http://www.snap.uaf.edu). Winter included December, January, and February; spring included March, April, and May; summer included June, July, and August; and fall included September, October, and November.

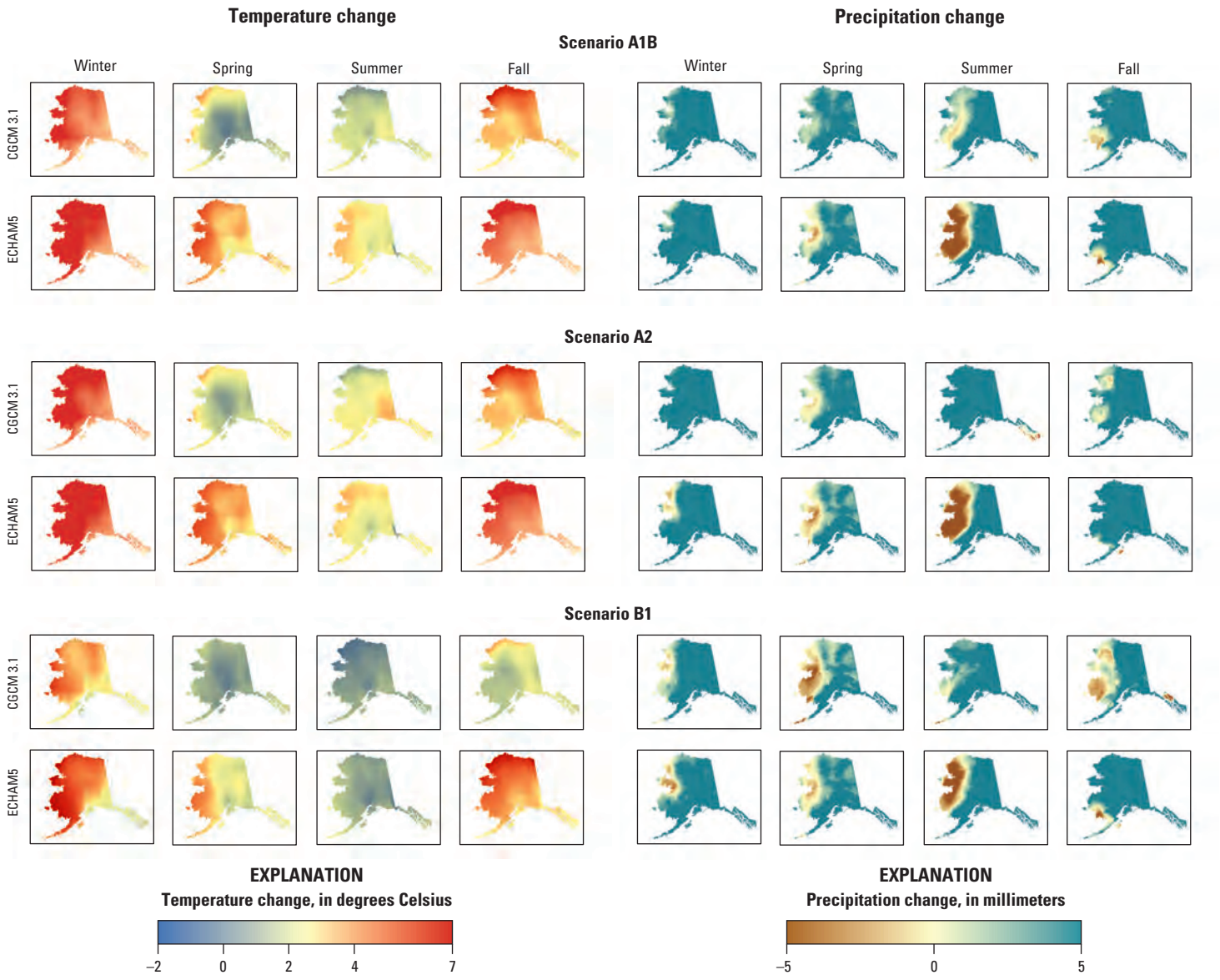

Figure 2.3. Projected changes in mean monthly temperature and total precipitation by season, calculated using the difference in mean values between 1980–2009 and 2070–2099 using downscaled data for version 3.1-T47 of the Canadian Centre for Climate Modelling and Analysis' Coupled Global Climate Model (CGCM3.1) and version 5 of the Max Planck Institute's European Centre Hamburg Model (ECHAM5) general circulation models and for the three scenarios A1B, A2, and B1 from the Intergovernmental Panel on Climate Change's Special Report on Emissions Scenarios (http://www.snap.uaf.edu). Winter included December, January, and February; spring included March, April, and May; summer included June, July, and August; and fall included September, October, and November.

Table 2.5. Summary statistics of projected changes in mean monthly temperature and total precipitation by season, calculated using the difference in mean values from 1980–2009 and 2070–2099 for each Landscape Conservation Cooperative (LCC) region and the full assessment domain (Alaska).

[Values represent the integration of all 1-kilometer pixels within the full assessment domain and individual subregions using downscaled data for the version 3.1-T47 of the Canadian Centre for Climate Modelling and Analysis' Coupled Global Climate Model (CGCM3.1) and version 5 of the Max Planck Institute's European Centre Hamburg Model (ECHAM5) general circulation models and for the three scenarios, B1, A1B, and A2, in order of low to high projected CO_2 emissions, from the Intergovernmental Panel on Climate Change's Special Report on Emissions Scenarios used in the assessment (http://www.snap.uaf.edu). Winter includes December, January, and February; spring includes March, April, and May; summer includes June, July, and August; and fall includes September, October, and November]

Season	Monthly temperature (degree Celsius)						Total precipitation (millimeter)					
	CGCM3.1			ECHAM5			CGCM3.1			ECHAM5		
	A1B	A2	B1	A1B	A2	B1	A1B	A2	B1	A1B	A2	B1
Arctic LCC												
Winter	6.36	8.09	3.55	8.03	8.19	4.93	8.42	9.55	6.81	9.94	7.08	5.25
Spring	2.55	2.46	1.26	3.78	3.96	2.53	5.30	4.82	2.45	4.33	3.72	3.99
Summer	1.25	1.79	0.23	2.76	2.94	1.08	6.75	14.73	8.04	3.73	3.10	4.03
Fall	4.92	5.77	2.58	7.21	7.51	5.56	9.59	7.39	5.96	18.39	20.08	16.53
Western Alaska LCC												
Winter	6.24	7.52	3.76	8.23	8.37	5.79	12.06	15.47	6.50	19.67	14.53	9.09
Spring	1.87	2.13	1.19	4.21	4.34	3.51	9.68	8.71	2.45	6.34	4.91	5.36
Summer	1.97	2.47	0.87	3.00	2.72	1.51	4.89	12.39	5.32	0.21	1.11	1.91
Fall	3.20	3.83	1.61	5.38	5.65	4.20	5.51	11.89	1.66	5.80	10.67	6.43
Northwest Boreal LCC North												
Winter	5.28	6.26	3.40	6.95	7.28	4.31	10.38	10.75	7.61	11.62	7.94	5.97
Spring	1.08	1.45	0.82	3.38	3.60	2.47	5.17	5.54	2.44	4.08	3.14	3.63
Summer	1.88	2.51	0.74	2.50	2.50	0.93	7.69	14.84	7.53	8.19	6.28	8.53
Fall	3.43	4.13	1.77	5.12	5.58	4.07	9.11	10.84	5.67	14.65	18.08	14.84
Northwest Boreal LCC South												
Winter	4.67	5.38	2.90	5.56	6.05	3.24	32.39	31.99	23.01	41.83	33.07	21.17
Spring	0.60	1.37	0.70	2.78	3.06	2.07	17.92	20.22	13.85	17.32	15.45	17.24
Summer	1.99	2.79	0.93	2.21	2.06	0.72	20.94	25.35	16.08	19.50	22.23	20.33
Fall	3.25	3.93	1.85	4.17	4.59	3.26	22.20	33.97	12.52	29.26	35.55	27.46
North Pacific LCC												
Winter	3.71	4.29	2.42	3.87	4.48	2.05	95.77	92.63	64.82	99.84	106.87	53.70
Spring	1.26	2.17	1.32	2.85	3.05	2.02	43.99	73.92	56.37	58.04	57.77	49.64
Summer	2.05	2.91	1.17	2.28	2.30	1.13	17.10	13.14	13.87	24.40	36.90	25.60
Fall	3.08	3.80	1.99	3.77	3.97	2.94	51.48	91.26	31.82	45.93	76.57	49.87
Alaska												
Winter	5.50	6.64	3.36	7.00	7.30	4.44	22.06	22.89	15.06	26.29	22.88	13.49
Spring	1.54	1.90	1.04	3.54	3.74	2.65	11.98	15.15	9.49	11.98	10.94	10.64
Summer	1.80	2.43	0.73	2.62	2.57	1.10	9.44	15.35	8.82	8.37	9.52	9.20
Fall	3.62	4.33	1.93	5.36	5.70	4.19	14.37	21.68	8.31	18.30	24.92	18.31

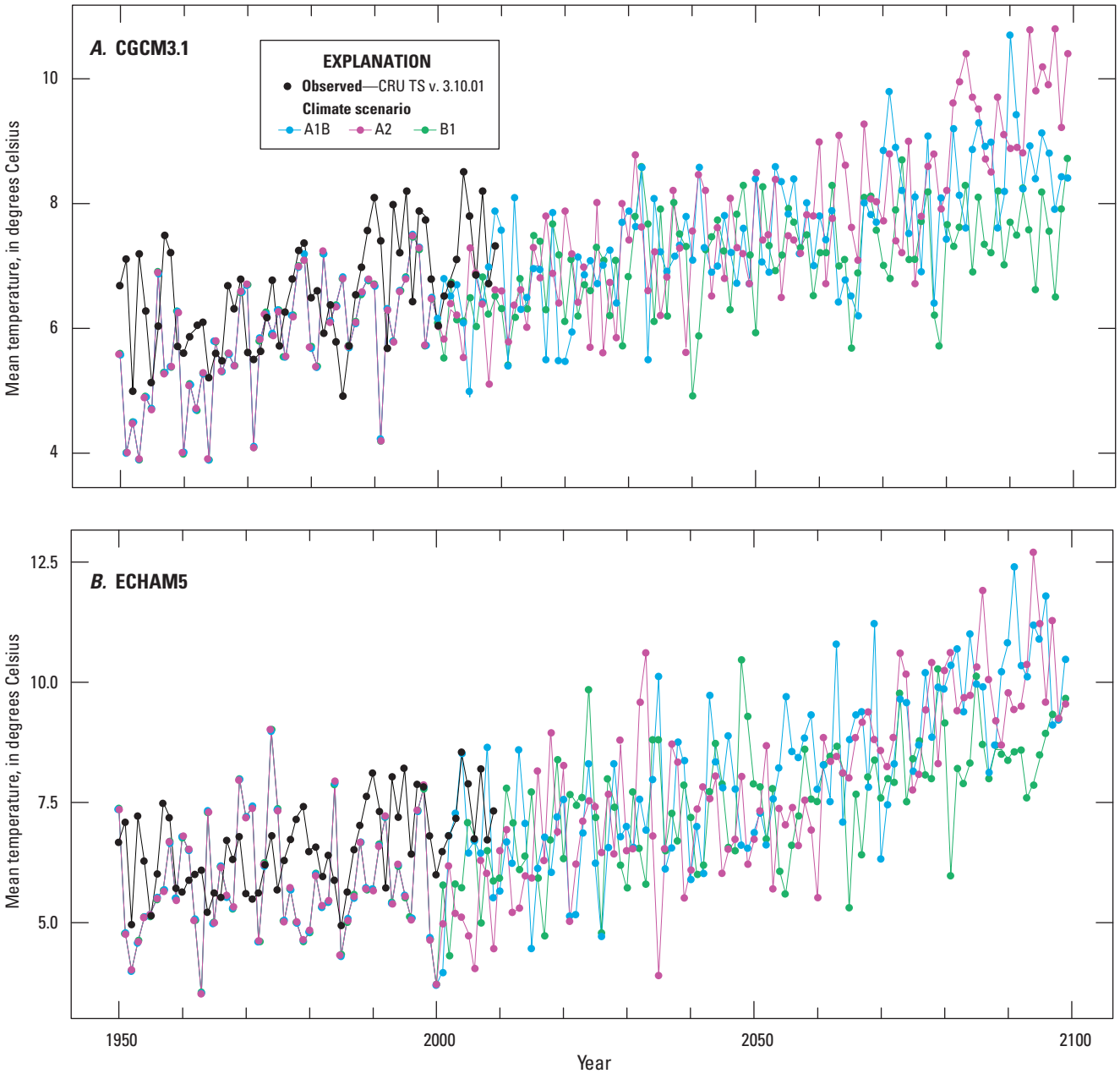

Figure 2.4. Projected growing season (April–September) mean temperature across the full assessment period (1950–2099). *A*, climate simulations by version 3.1-T47 of the Canadian Centre for Climate Modelling and Analysis' Coupled Global Climate Model (CGCM3.1) and *B*, climate simulations by version 5 of the Max Planck Institute's European Centre Hamburg Model (ECHAM5). Historical observations are from the Climate Research Unit time series CRU TS v. 3.10.01. Climate scenarios A1B, A2, and B1 from the Intergovernmental Panel on Climate Change's Special Report on Emissions Scenarios.

smaller than the differences among scenarios. Portions of western Alaska are projected to increase the least and some areas would likely experience some seasonal decreases in spring and summer (fig. 2.3). Regional trends varied considerably among climate simulations, with the CGCM3.1 model projecting slightly larger increases for the A1B scenario than for the A2 scenario. In contrast, the ECHAM5 model projected slightly larger increases for the A2 scenario than for the A1B scenario. Of the simulations, that for scenario B1 with ECHAM5 produced the largest seasonal increases in precipitation in spring (March, April, May) and summer (June, July, August).

2.4.4. Projected Land Cover

The projected changes in land cover varied substantially across the assessment domain, but varied little across GCM climate scenarios (table 2.6). Differences between the GCMs were minimal except for the Arctic LCC. Change was defined as the percentage of the domain that changed land-cover type at least once over the projection period (2010–2099). Total projected land-cover change across the full domain ranged from a low of 56.5 percent in the B1 scenario of the CGCM3.1 model to a high of 61.2 percent in the A1B scenario of the ECHAM5 model. The greatest amount of change occurred within the Northwest Boreal LCC North (approximately 97.5 percent in both models) and the least amount of change, not including the primarily static North Pacific LCC, was simulated in the Arctic LCC (ranging from 30 to 46 percent for the CGCM3.1 and ECHAM5 models, respectively) (fig. 2.5).

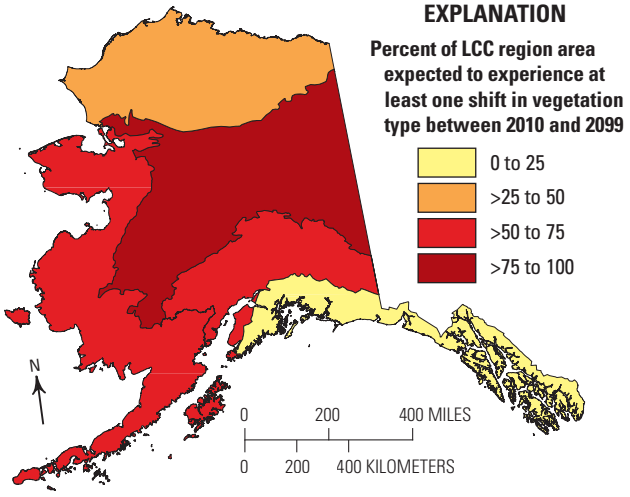

Figure 2.5. Projected land-cover change footprint visualized by Landscape Conservation Cooperative (LCC) region. This visualization is for the version 3.1-T47 of the Canadian Centre for Climate Modelling and Analysis' Coupled Global Climate Model (CGCM3.1) general circulation model, but the version 5 of the Max Planck Institute European Centre Hamburg Model (ECHAM5) model produces the same results for the binned categories depicted, and the results are also consistent across climate change scenarios A1B, A2, and B1 from the Intergovernmental Panel on Climate Change's Special Report on Emissions Scenarios. Finer differences between the two general circulation models and the three climate change scenarios are presented in table 2.6. Change was defined as the portion of the domain that changed cover type at least once over the projection period (2010–2099).

Table 2.6. Projected land-cover-change footprint for the Landscape Conservation Cooperative (LCC) regions and the full assessment domain (Alaska).

[Change was defined as the percentage of the domain that changed land-cover type at least once over the projection period (2010–2099). This assessment used downscaled data for two general circulation models, version 3.1-T47 of the Canadian Centre for Climate Modelling and Analysis' Coupled Global Climate Model (CGCM3.1) and version 5 of the Max Planck Institute's European Centre Hamburg Model (ECHAM5), and three scenarios, B1, A1B, and A2, in order of low to high projected CO_2 emissions, from the Intergovernmental Panel on Climate Change's Special Report on Emissions Scenarios. km^2, square kilometer]

LCC region	Area (km^2)	Land-cover change (percent)					
		CGCM3.1			ECHAM5		
		A1B	A2	B1	A1B	A2	B1
Arctic LCC	308,593	33.5	38.8	30.8	46.2	43.7	41.8
Western Alaska LCC	378,221	55.7	56.1	52.9	58.0	57.6	56.5
Northwest Boreal LCC North	456,584	97.5	97.5	97.4	97.5	97.5	97.5
Northwest Boreal LCC South	186,303	55.3	56.0	54.9	56.2	56.0	55.4
North Pacific LCC	163,361	0.9	0.9	0.9	0.9	0.9	0.9
Alaska	**1,493,062**	**57.8**	**59.1**	**56.5**	**61.2**	**60.5**	**59.8**

Projected land-cover changes across the full assessment domain between 2009 and 2099 occurred within both the forest and tundra types (table 2.7, fig. 2.6). No changes were projected in land cover for coastal temperate forest, heath tundra, or wetland tundra owing to the static nature in which the vegetation succession model treats these land-cover types. Model results for the full assessment domain indicated projected decreases in late successional white and black spruce forests and concomitant increase in early successional deciduous forest across GCMs and climate scenarios with the magnitudes of change being greatest for the ECHAM5 simulations. The exception was the simulation under scenario B1 with CGCM3.1, which projected a small increase in black spruce forest (1.9 percent) and a moderate increase in white spruce forest (12.1 percent). Forest land-cover changes were greatest under the A2 scenario with the CGCM3.1 model, but were greatest under the A1B scenario with the ECHAM5 model. The CGCM3.1 simulations projected a consistent decreases in both graminoid and shrub tundra, whereas the ECHAM5 simulations projected moderate decreases in graminoid tundra (20–26 percent) but increases in shrub tundra (4–8 percent).

Consistent decreases in white and black spruce forests and concomitant increases in deciduous forest were projected for all regions and scenarios under the ECHAM5 simulations (table 2.7). Projected decreases were greatest under the A1B scenario and smallest under the B1 scenario. For the CGCM3.1 simulations, the model results varied among regions and scenarios. The magnitude of change was greatest under the A2 scenario except for the Western Alaska LCC. Within the boreal-forest-dominated Northwest Boreal LCC North and South, the B1 scenario projected small increases in spruce forests whereas the A2 scenario projected moderate decreases. The A1B scenario produced opposite trends with small increases in spruce forests projected for the Northwest Boreal LCC South and small decreases projected for the Northwest Boreal LCC North.

Although the Arctic and Western Alaska LCCs are both dominated by tundra, projected changes in tundra land cover exhibited opposite trends consistently across GCMs and scenarios. For the Arctic LCC, decreases in graminoid tundra and increases in shrub tundra were projected, with a greater magnitude of change under the ECHAM5 simulations. For the Western Alaska LCC, in contrast, increases in graminoid tundra and decreases in shrub tundra were projected, with a greater magnitude of change under the CGCM3.1 simulations.

In the Arctic LCC, white spruce forest was projected to increase (18.2–66.3 percent) whereas black spruce forest was projected to decrease (8.4–36.1 percent) under the CGCM3.1 simulations with the magnitude of change greatest under the B1 scenario for white spruce and under the A2 scenario for black spruce (table 2.7). In contrast, both white and black spruce forests were projected to decrease (24.9–63.6 percent) under the ECHAM5 simulations with the magnitude of the decreases greatest under the A2 scenario and smallest under the B1 scenario. For all simulations, graminoid tundra was projected to decrease (8.4–23.6 percent), whereas shrub tundra was projected to increase (2.1–21.3 percent). Projected changes in tundra land cover were slightly greater under the A1B scenario than the A2 scenario and the least amount of change was projected under the B1 scenario.

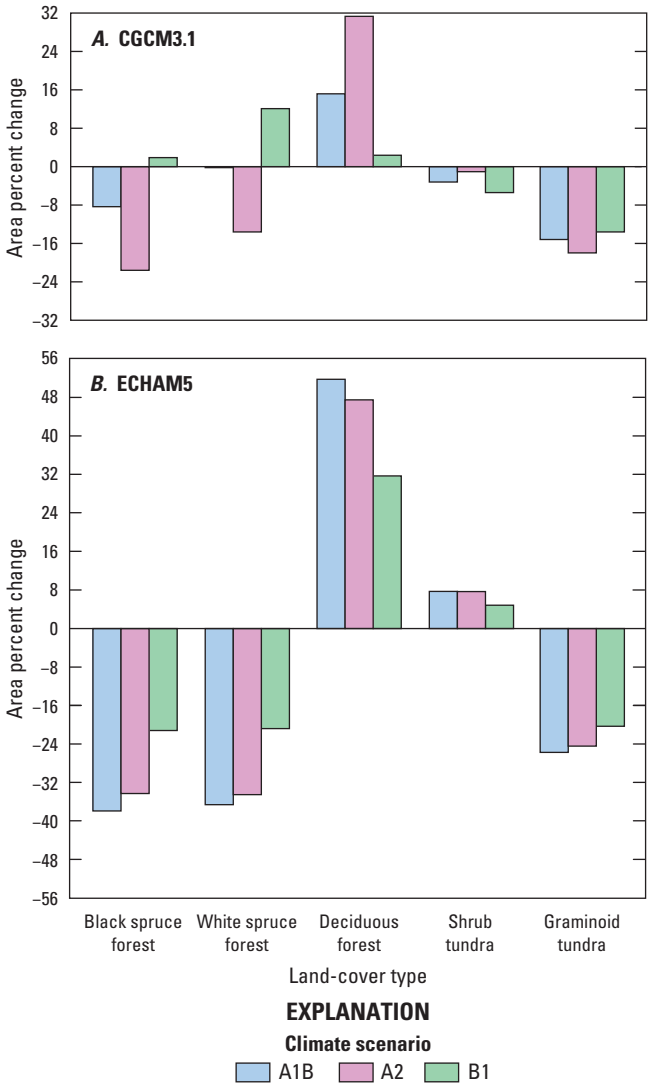

Figure 2.6. Projected land-cover change between 2009 and 2099 across the full assessment domain under the three emissions scenarios A1B, A2, and B1 of the Intergovernmental Panel on Climate Change's Special Report on Emissions Scenarios. *A*, changes projected by version 3.1-T47 of the Canadian Centre for Climate Modelling and Analysis' Coupled Global Climate Model (CGCM3.1) climate simulations and *B*, changes projected by version 5 of the Max Planck Institute's European Centre Hamburg Model (ECHAM5) climate simulations.

In the Western Alaska LCC, white and black spruce forests were projected to decrease (12.0–45.6 percent) under all simulations, except for the CGCM3.1 simulation under the B1 scenario, which resulted in a 6.4-percent projected increase in white spruce forest (table 2.7). Graminoid tundra was projected to increase (0.4–9.2 percent) across all simulations. In contrast, shrub tundra was projected to decrease (3.6–11.3 percent) across all simulations.

Table 2.7. Projected change in land-cover type between the end of the historical period (2009) and the end of the projection period (2099) for each Landscape Conservation Cooperative (LCC) region and the full assessment domain (Alaska).

[Heath tundra, wetland tundra, and coastal temperate forest are not presented due to the static nature of these cover types in the Alaska Frame-Based Ecosystem Code (ALFRESCO) model. This assessment used downscaled data for two general circulation models, version 3.1-T47 of the Canadian Centre for Climate Modelling and Analysis' Coupled Global Climate Model (CGCM3.1) and version 5 of the Max Planck Institute's European Centre Hamburg Model (ECHAM5), and three scenarios, B1, A1B, and A2, in order of low to high projected CO_2 emissions, from the Intergovernmental Panel on Climate Change's Special Report on Emissions Scenarios. NA, not applicable]

Land-cover type	Change in land-cover type (percent)					
	CGCM3.1			ECHAM5		
	A1B	A2	B1	A1B	A2	B1
Arctic LCC						
Black spruce forest	–19.7	–36.1	–8.4	–63.0	–63.6	–54.7
White spruce forest	49.8	18.2	66.3	–36.8	–46.1	–24.9
Deciduous forest	232.5	396.8	129.1	620.4	598.3	527.0
Shrub tundra	4.2	8.9	2.1	21.3	20.6	13.8
Graminoid tundra	–10.2	–14.4	–8.4	–23.6	–22.1	–16.4
Western Alaska LCC						
Black spruce forest	–24.9	–29.4	–12.0	–45.6	–43.1	–33.6
White spruce forest	–11.6	–16.1	6.4	–40.5	–40.3	–30.6
Deciduous forest	63.1	73.7	34.0	106.0	102.6	81.4
Shrub tundra	–9.5	–9.8	–11.3	–4.4	–3.6	–3.6
Graminoid tundra	8.2	9.2	6.6	3.9	3.7	0.4
Northwest Boreal LCC North						
Black spruce forest	–8.0	–25.9	3.0	–43.9	–34.1	–13.6
White spruce forest	–7.9	–24.3	3.7	–41.9	–33.8	–12.2
Deciduous forest	24.5	69.2	–5.1	113.0	91.4	34.8
Shrub tundra	1.8	1.5	1.0	4.5	5.0	4.7
Graminoid tundra	–49.7	–46.3	–46.1	–45.6	–44.3	–44.0
Northwest Boreal LCC South						
Black spruce forest	1.3	–15.2	9.6	–30.2	–27.4	–14.9
White spruce forest	4.4	–10.9	13.9	–32.6	–30.5	–18.7
Deciduous forest	3.0	15.4	–3.9	29.1	27.5	17.4
Shrub tundra	–17.5	–13.6	–25.1	3.9	1.9	3.2
Graminoid tundra	–72.6	–69.9	–71.4	–67.9	–66.5	–67.9
North Pacific LCC						
Black spruce forest	–6.4	–9.5	–1.9	–20.0	–13.4	–4.3
White spruce forest	–7.2	–10.0	–1.6	–19.4	–14.9	–3.6
Deciduous forest	90.0	127.3	20.9	248.2	174.5	53.2
Shrub tundra	0.0	0.0	0.0	0.0	0.0	0.0
Graminoid tundra	NA	NA	NA	NA	NA	NA
Alaska						
Black spruce forest	–8.3	–21.6	1.9	–37.8	–34.2	–21.1
White spruce forest	–0.2	–13.6	12.1	–36.5	–34.4	–20.7
Deciduous forest	15.2	31.3	2.4	51.6	47.4	31.6
Shrub tundra	–3.2	–1.0	–5.4	7.7	7.7	4.8
Graminoid tundra	–15.2	–18.0	–13.6	–25.7	–24.4	–20.2

In the Northwest Boreal LCC North, white and black spruce forests were projected to decrease substantially (7.9–43.9 percent) under all simulations, except for the simulations under the B1 scenario, which resulted in minimal increases of approximately 3 percent (table 2.7). Graminoid tundra was also projected to decrease (44.0–49.7 percent) under all simulations. In contrast, shrub tundra was projected to increase (1.0–5.0 percent) under all simulations.

In the Northwest Boreal LCC South, small to moderate changes (that varied from decreases to increases) were projected in white and black spruce forests across the scenarios with CGCM3.1 (table 2.7). In contrast, decreases in white and black spruce forests were projected for all scenarios with ECHAM5. Graminoid and shrub tundra were projected to decrease (13.6–72.6 percent) under the CGCM3.1 simulations. However, under the ECHAM5 simulations graminoid tundra was projected to decrease (66.5–67.9 percent), whereas shrub tundra was projected to increase minimally (1.9–3.9 percent).

Because ALFRESCO does not model changes in temperate forest types, projected land-cover changes were minimal in the North Pacific LCC where this land-cover type is dominant. For the small amount of spruce forest land-cover types found within this LCC, both white and black spruce forests were projected to decrease (1.6–20.0 percent) under all simulations.

Distributional trends across the full assessment domain revealed projected decreases in area of spruce forest land cover across all simulations (fig. 2.7). These decreases were greatest for the ECHAM5 simulations. An associated increase in early successional deciduous forest was projected under all simulations. Graminoid tundra was also projected to decrease in area across all simulations. In contrast, the area of shrub tundra was projected to be relatively stable under the CGCM3.1 simulations, whereas a small increase was projected under the ECHAM5 simulations.

Distributional trends among the LCC regions varied substantially (figs. 2.8 through 2.12). In the Arctic LCC, all simulations projected decreases in graminoid tundra and increases in shrub tundra (fig. 2.8). Under the CGCM3.1 simulations, a small increase in white spruce forest was projected.

The Western Alaska LCC exhibited similar results to its tundra-dominated Arctic LCC counterpart for forest land-cover types, but opposite trends for the tundra land-cover types (fig. 2.9). In contrast to the Arctic LCC, the Western Alaska LCC simulations projected variable but decreasing shrub tundra trends across all simulations. Under the CGCM3.1 simulations, graminoid tundra was projected to increase slightly whereas under the ECHAM5 simulations, an increase at the beginning of the century was projected, followed by a decline ending in areal extents similar to beginning levels.

The simulations for the Northwest Boreal LCC North projected moderate to large changes in forest distribution (fig. 2.10). For the CGCM3.1 simulations, white and black spruce forest extent was projected to vary from moderate decreases under the A2 scenario to small increases under the B1 scenario. In contrast, the ECHAM5 simulations projected large decreases in white and black spruce forest extent across all scenarios, with concomitant increases in early successional deciduous forest. Graminoid tundra was projected to decrease in all simulations. Projected changes in shrub tundra extent were opposite for the GCMs, with projected decreases under CGCM3.1 but increases under ECHAM5.

The projections for the Northwest Boreal LCC South mirrored the trends exhibited in the Northwest Boreal LCC North, except that under the CGCM3.1 simulations shrub tundra was projected to increase across all scenarios—in contrast to the CGCM3.1 simulations for the Northwest Boreal LCC North (fig. 2.11). In all simulations, the projected areal extent of change was substantially smaller than for the Northwest Boreal LCC North.

The simulations for the North Pacific LCC projected only minor changes owing to the static nature of the major ecosystem type (coastal temperate forest) in ALFRESCO. Along the extreme northern portions of this LCC, minor decreases in spruce forests were projected with concomitant increases in deciduous forest (fig. 2.12). These trends were consistent across all simulations.

2.4.5. Projected Wildfire

2.4.5.1. Retrospective Simulations

Calibration simulations were performed to tune the modeled relationship between climate and fire. Calibrations iteratively adjusted the quantitative linkage between climate and fire by comparing model output (such as, fire numbers and extent, stand age structure) to the corresponding historical data. Several metrics were used to calibrate the performance of ALFRESCO simulations (Rupp and others, 2000, 2002, 2006, 2007). These metrics included (1) the frequency-area distribution of the fire sizes, (2) the inter-annual variability from 1950 through 2009, and (3) the mean area burned from 1950 through 2009. Calibration results are not presented here but followed the methods outlined in Mann and others (2012). Once a sufficient correspondence between the historical data and the simulation output was obtained across multiple metrics, the calibration optimization was halted.

ALFRESCO simulations of the historical period of record provided reasonable depictions of the fire regime in Alaska. Specifically, the frequency-area distribution, inter-annual variability in area burned, and spatial distribution of fires were consistent with those from the observed record. To account for stochastic components of the fire regime (such as, ignitions, duration of vegetation dominance through succession, and so forth), multiple replicates (n=200) of fire activity and subsequent succession were simulated. Projected model results were then assembled and distributional properties across replicates were analyzed. The model performed relatively well in simulating historical wildfire activity driven by historical climate data (table 2.8). The simulated number of wildfires averaged 60 per year, ranging from 48 to 78.

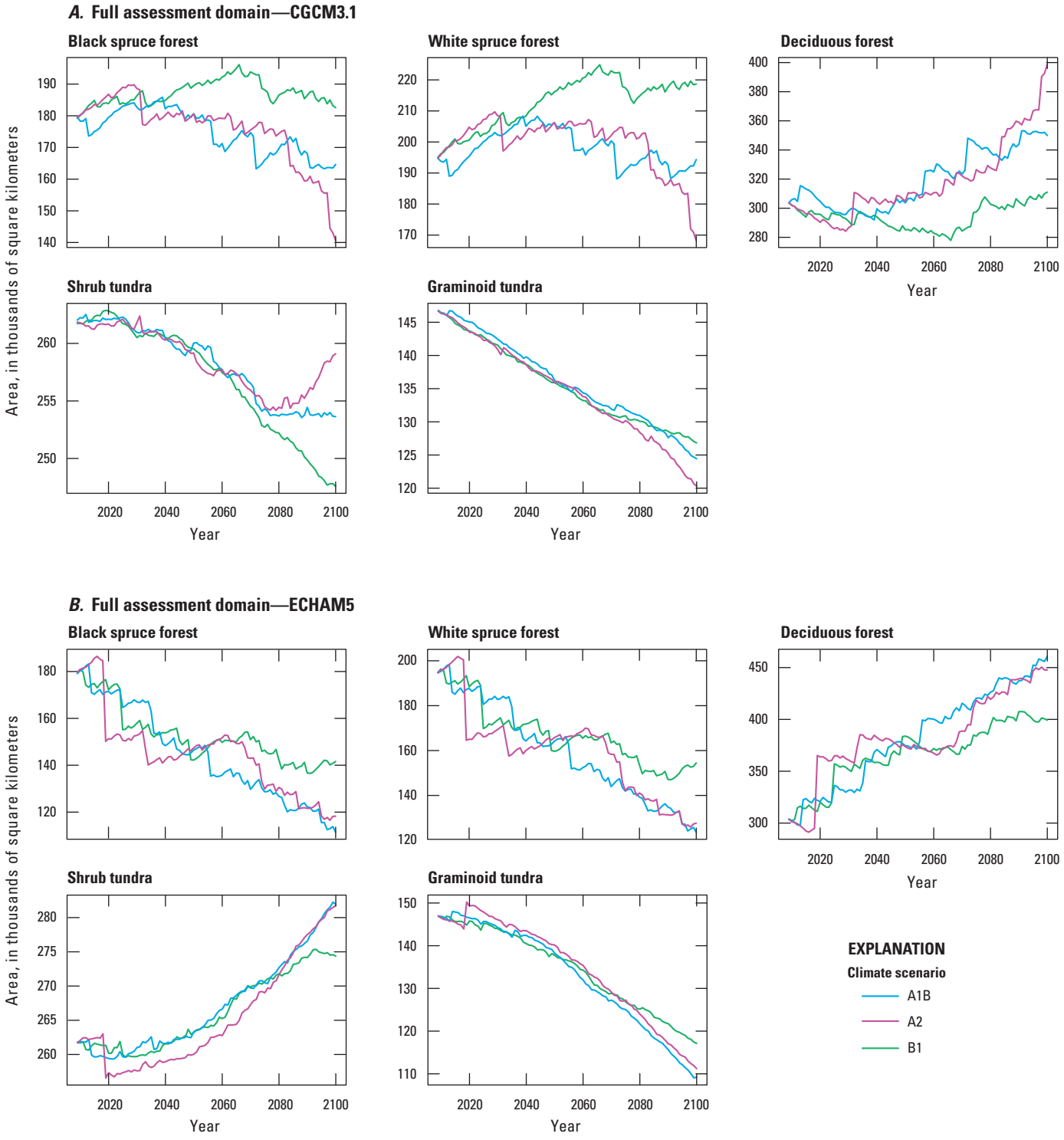

Figure 2.7. Projected change in land-cover type from 2009 through 2099 across the full assessment domain. *A*, changes projected by version 3.1-T47 of the Canadian Centre for Climate Modelling and Analysis' Coupled Global Climate Model (CGCM3.1) climate simulations and *B*, changes projected by version 5 of the Max Planck Institute's European Centre Hamburg Model (ECHAM5) climate simulations under the three emissions scenarios A1B, A2, and B1 of the Intergovernmental Panel on Climate Change's Special Report on Emissions Scenarios. Heath tundra, wetland tundra, and coastal temperate forest land-cover types are not presented owing to the static nature of these land-cover types in the Alaska Frame-Based Ecosystem Code (ALFRESCO) model.

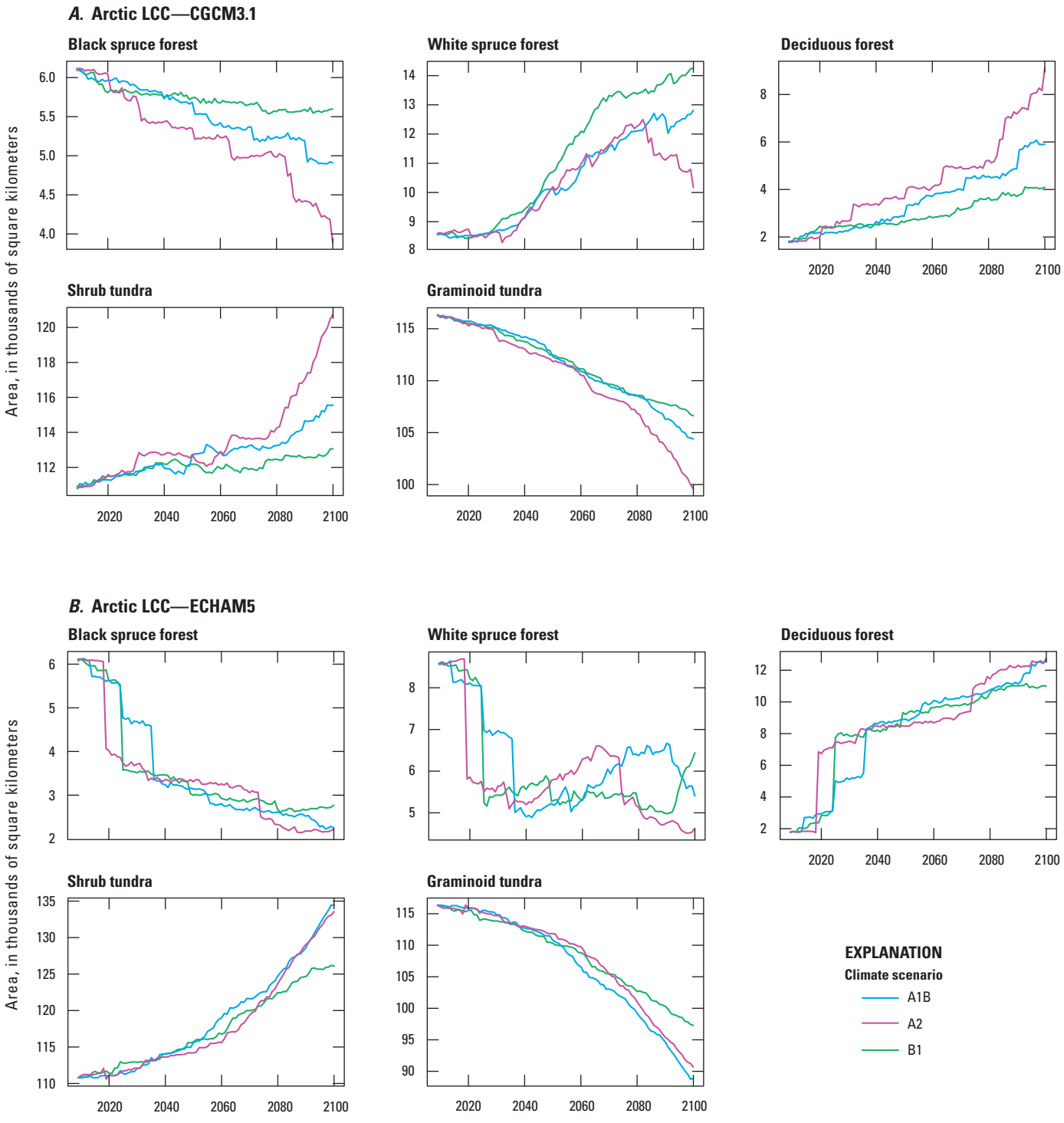

Figure 2.8. Projected change in land-cover type from 2009 through 2099 across the Arctic Landscape Conservation Cooperative (LCC). Details regarding the simulations of land-cover change shown can be found in figure 2.7.

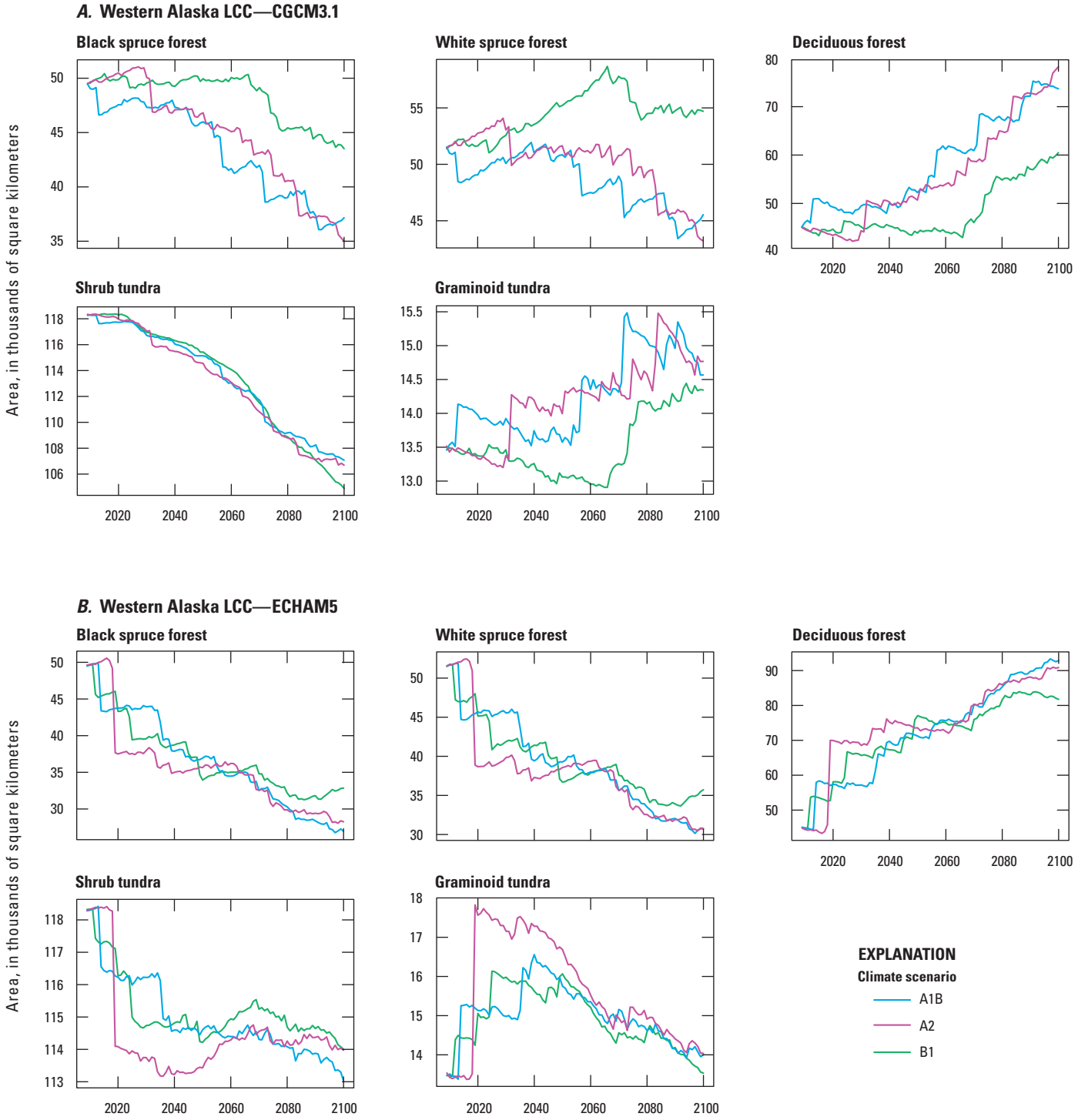

Figure 2.9. Projected change in land-cover type from 2009 through 2099 across the Western Alaska Landscape Conservation Cooperative (LCC). Details regarding the simulations of land-cover change shown can be found in figure 2.7.

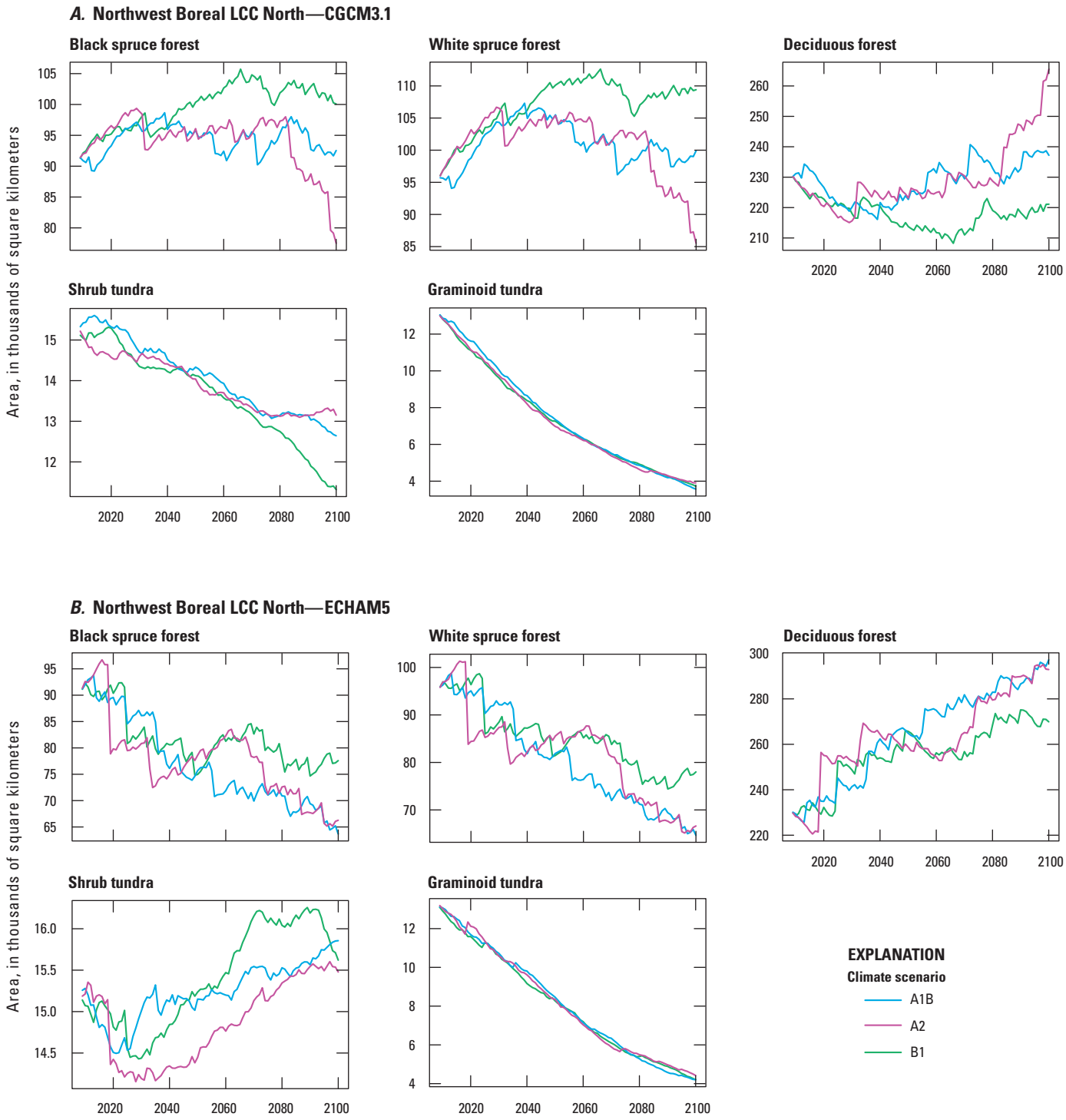

Figure 2.10. Projected change in land-cover type from 2009 through 2099 across the Northwest Boreal Landscape Conservation Cooperative (LCC) North. Details regarding the simulations of land-cover change shown can be found in figure 2.7.

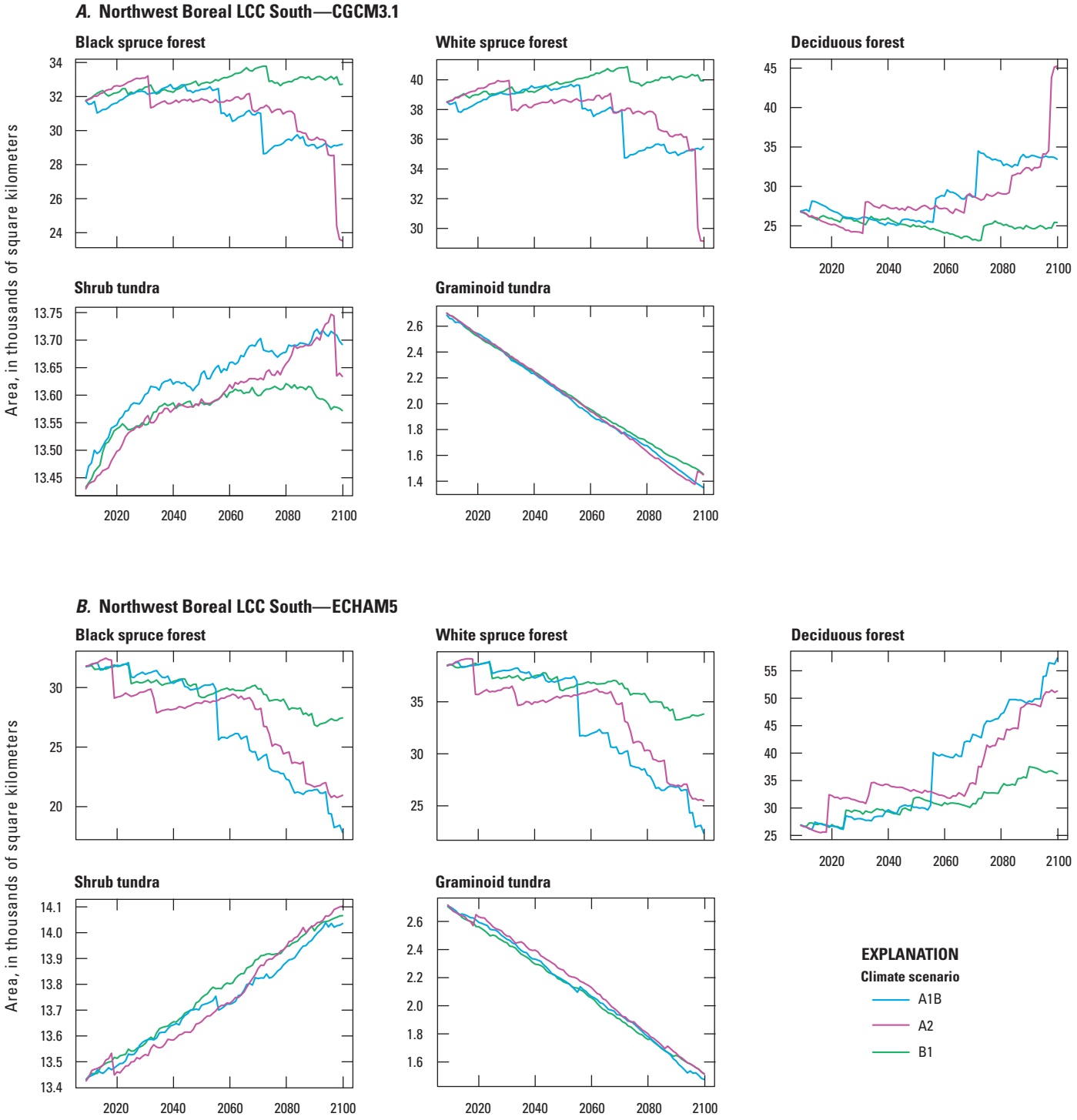

Figure 2.11. Projected change in land-cover type from 2009 through 2099 across the Northwest Boreal Landscape Conservation Cooperative (LCC) South. Details regarding the simulations of land-cover change shown can be found in figure 2.7.

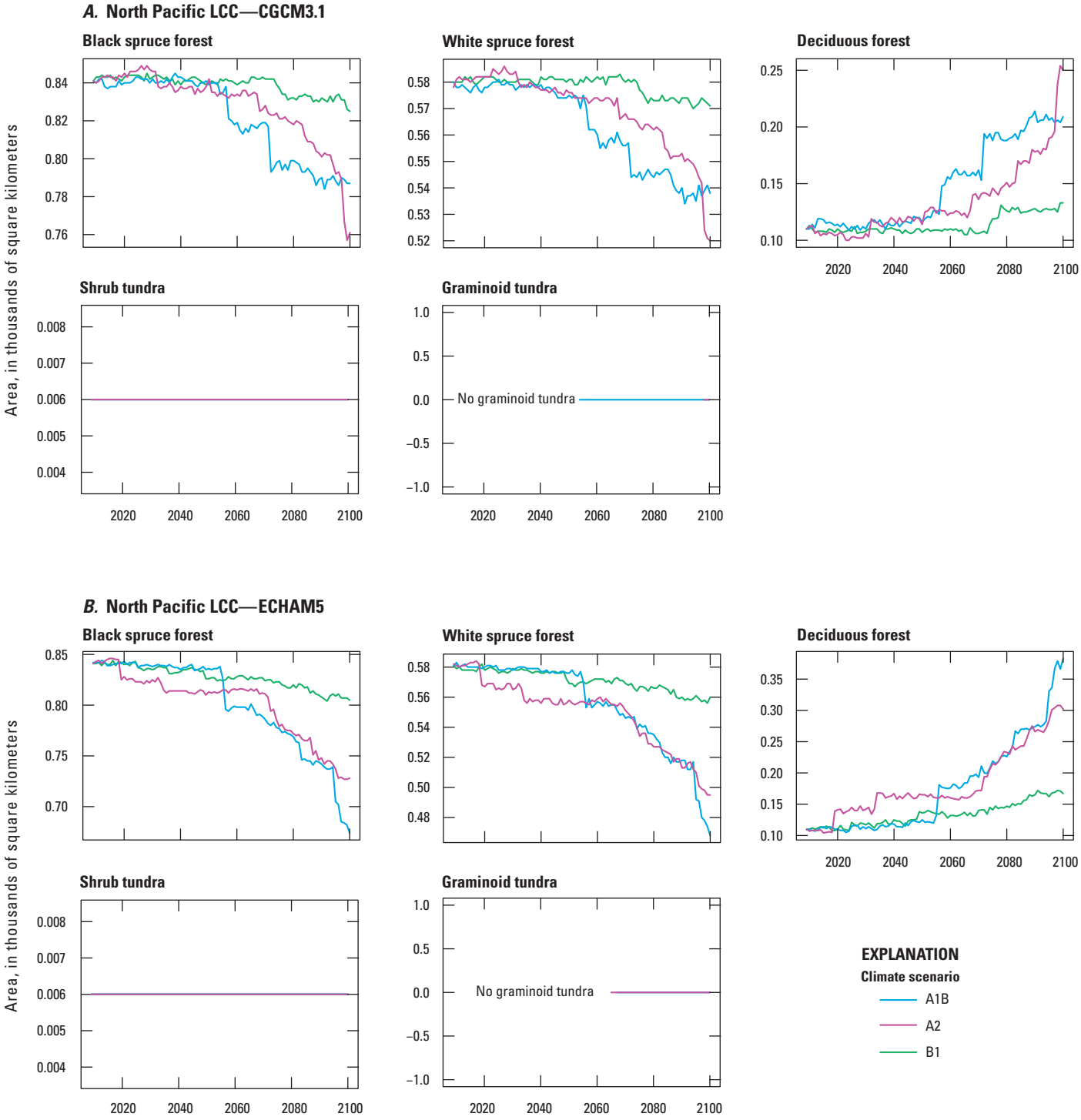

Figure 2.12. Projected change in land-cover type from 2009 through 2099 across the North Pacific Landscape Conservation Cooperative (LCC). Details regarding the simulations of land-cover change shown can be found in figure 2.7.

Table 2.8. Observed and simulated fire data from Alaska Frame-Based Ecosystem Code (ALFRESCO) model for each Landscape Conservation Cooperative (LCC) region and the full assessment domain (Alaska) during the baseline period (1950–2009).

[Summary statistics are based on 200 model replicates. km^2, square kilometer; —, not applicable]

Metric	Observed		Simulated	
	Number of wildfires per year	Annual area burned (km^2)	Number of wildfires per year	Annual area burned (km^2)
Arctic LCC				
Mean	2.1	60.49	0.9	86
Standard deviation	3.2	178.16	0.3	210
Minimum	0	0	0	2
Median	0	0	1	10
Maximum	13	1,106.82	2	1,130
Year of maximum	2005	2007	—	—
Western Alaska LCC				
Mean	5.82	393.81	8	762
Standard deviation	7.68	1,258.46	2	1,168
Minimum	0	0	5	23
Median	3.5	33.42	8	255
Maximum	37	8,313.50	12	6,411
Year of maximum	1972	1957	—	—
Northwest Boreal LCC North				
Mean	31.8	3,262.26	44	2,802
Standard deviation	33.07	5,178.67	5	3,089
Minimum	0	0	35	335
Median	20	1,296.82	43	1,612
Maximum	137	26,683.54	57	13,983
Year of maximum	2005	2004	—	—
Northwest Boreal LCC South				
Mean	2.15	54.49	10	331
Standard deviation	2.7	112.52	2	441
Minimum	0	0	6	31
Median	1	4.28	9	187
Maximum	15	615.4	14	2,059
Year of maximum	2009	2009	—	—
North Pacific LCC				
Mean	0.6	2.21	0.1	4
Standard deviation	0.92	6.93	0.2	2
Minimum	0	0	0	1
Median	0	0	0	3
Maximum	4	36.31	1	11
Year of maximum	1991	1991	—	—
Alaska				
Mean	41.3	3,791.50	60	3,789
Standard deviation	41.92	5,709.97	7	4,343
Minimum	0	0	48	433
Median	27	1,596.77	59	2,028
Maximum	176	27,071.72	78	18,391
Year of maximum	2005	2004	—	—

The average number of simulated fires is slightly higher than the historical average; however, the estimate of the average for the historical data is likely biased low owing to under-reporting in the first decade of the observational record. Historical annual area burned averaged 3,791 km^2 (table 2.4)—that is, 0.25 percent of the total area of the Alaska simulation domain, which has a total area of 1.49 million km^2. Simulation results for that same period had an average annual area burned of 3,789 km^2. The inter-annual variability of the simulated fire activity was smaller than that of the historical data. This is largely due to deficiencies in the model's ability to depict inter-annual variability in the ignitions because of a lack of reliable historical data regarding ignitions.

2.4.5.2. Future Simulations

The simulation results of fire activity for the last decade of the projection period (2090–2099) were compared with simulated results from the most recent full decade (2000–2009), referred to as the historical reference period. Results are summarized using percentiles from the distribution of output (such as, number of wildfires, area burned) across 200 model replicates for each simulation. Greater differences were found between simulated output from GCMs across all emissions scenarios than among emissions scenarios within a given GCM. Across the full domain of this assessment and across all simulations, the median (across 200 model replicates) projected number of wildfires for 2090–2099 ranged from 51 to 88 (table 2.9, fig. 2.13). The projected annual area

Table 2.9. Summary of fire activity for the full assessment domain simulated for the last decades of the historical period (2000–2009) and the projection period (2090–2099).

[The 50th (median) and 95th percentiles were computed across 200 model replicates for each future climate simulation. The six simulations were combinations of the two general circulation models, version 3.1-T47 of the Canadian Centre for Climate Modelling and Analysis' Coupled Global Climate Model (CGCM 3.1; McFarlane and others, 1992; Flato, 2005) and version 5 of the Max Planck Institute's European Centre Hamburg Model (ECHAM5; Roeckner and others, 2003, 2004), and three climate change scenarios, B1, A1B, and A2, in order of low to high projected CO_2 emissions, of the Intergovernmental Panel on Climate Change's Special Report on Emissions Scenarios (Nakićenović and Swart, 2000). km^2, square kilometer]

Climate scenario	Metric (percentile)	Historical period		Projection period		Change in number of wildfires (percent)	Change in area burned (percent)
		Number of wildfires	Area burned (km^2)	Number of wildfires	Area burned (km^2)		
CGCM3.1							
A1B	Median	60	3,398	60	2,887	0.8	–15.0
A1B	95th	84	17,971	84	19,259	0.9	7.2
A2	Median	59	3,155	62	5,324	4.2	68.8
A2	95th	84	17,880	88	32,569	5.2	82.2
B1	Median	59	3,089	66	3,636	12.7	17.7
B1	95th	84	17,667	88	16,038	4.8	–9.2
ECHAM5							
A1B	Median	59	3,135	55	4,904	–6.8	56.4
A1B	95th	85	18,079	83	25,677	–2.5	42.0
A2	Median	59	3,060	51	3,412	–13.6	11.5
A2	95th	84	17,579	79	23,435	–5.9	33.3
B1	Median	59	3,159	53	2,576	–10.2	–18.5
B1	95th	85	17,428	75	11,429	–11.4	–34.4

burned across 200 model replicates averaged 12,591 km^2, or 0.85 percent of the assessment domain, which has a total area of 1.49 million km^2. The median (across 200 model replicates) annual area burned ranged from 2,477 km^2 (0.16 percent of total area) to 33,039 km^2 (2.2 percent of total area).

Under the CGCM3.1 simulations, the 50th (median) and 95th percentiles for the number of wildfires were projected to increase across all scenarios (table 2.9, fig. 2.13*A*). The increases for both percentiles were least pronounced and somewhat negligible under the A1B scenario. Projections of future area burned varied in magnitude and direction of change (relative to present) across scenarios. The 50th percentile of area burned for the B1 and A2 scenarios was projected to increase by 17.7 percent and 68.8 percent, respectively. In contrast, the 50th percentile of area burned for the A1B scenario was projected to decrease by 15 percent. The 95th percentile of area burned was projected to increase for the A1B and A2 scenarios by 7.2 percent and 82.2 percent, respectively. In contrast, the 95th percentile of area burned for the B1 scenario was projected to decrease by 9.2 percent.

Under the ECHAM5 simulations, the 50th and 95th percentiles for the number of wildfires were projected to decrease across all scenarios (table 2.9, fig. 2.13*B*), with the greatest projected decrease under the A2 scenario and the smallest projected decrease under the B1 scenario. The area burned was projected to increase for the A1B and A2 scenarios; in contrast, the area burned was projected to decrease for the B1 scenario. The greatest change from present was projected under the A1B scenario, with 56-percent and 42-percent increases for the 50th and 95th percentiles of area burned, respectively.

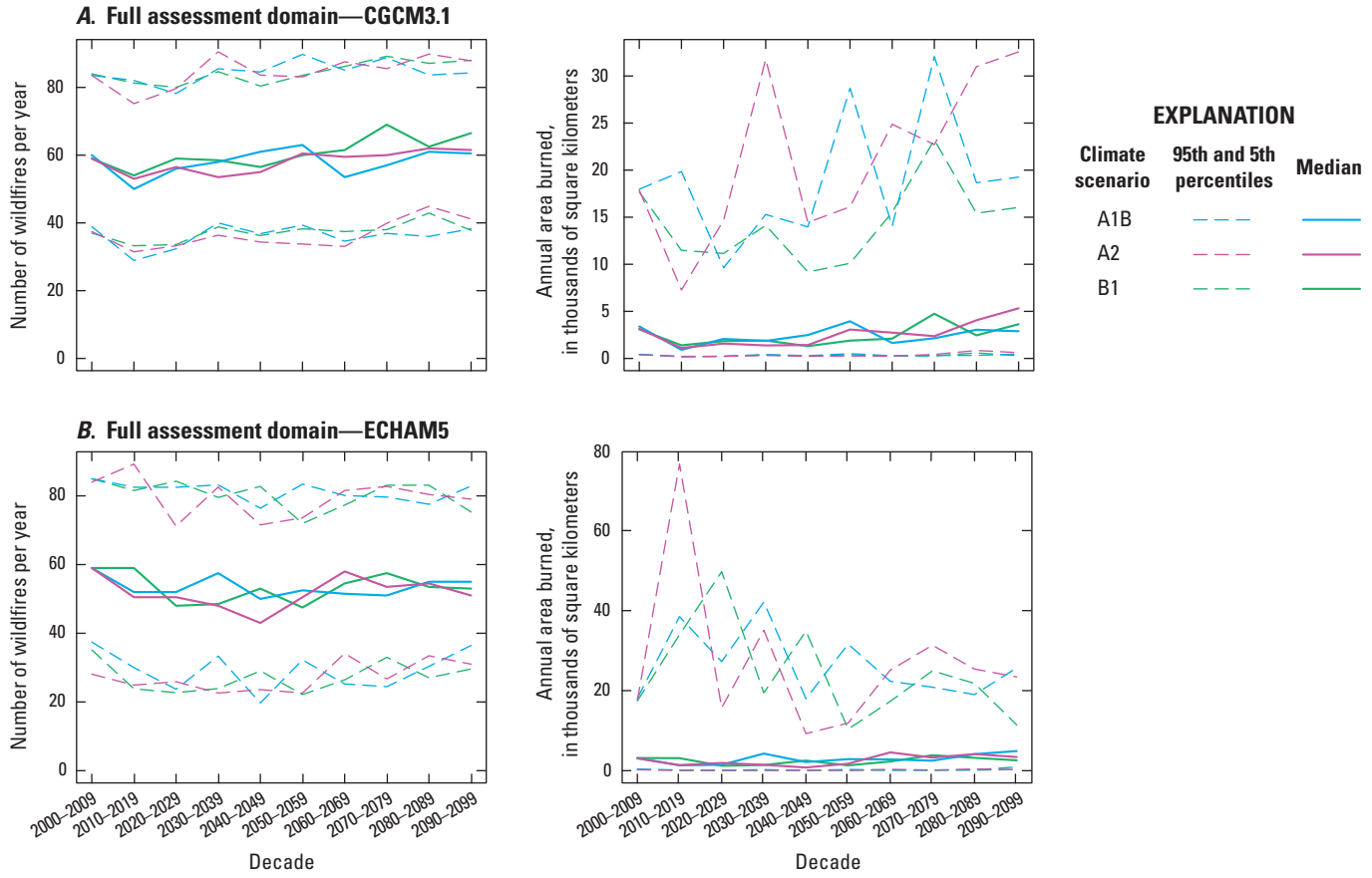

Figure 2.13. Simulated fire activity showing decadal summaries of annual projected number of wildfires and area burned for each decade from 2000 through 2099 across the full assessment domain for the *A*, version 3.1-T47 of the Canadian Centre for Climate Modelling and Analysis' Coupled Global Climate Model (CGCM3.1) simulation and *B*, version 5 of the Max Planck Institute's European Centre Hamburg Model (ECHAM5) simulation. The 50th (median), 5th, and 95th percentiles were computed across 200 simulations for climate change scenarios A1B, A2, and B1 of the Intergovernmental Panel on Climate Change's Special Report on Emissions Scenarios.

The Northwest Boreal LCC North had the most (approximately 85 percent of the statewide total) historical fire activity among the five LCC regions of the assessment and was also projected to have the most future fire activity. Under the CGCM3.1 simulations, the 50th and 95th percentiles for the number of wildfires were projected to increase for all scenarios (table 2.10, fig. 2.14*A*). The projected magnitude and direction of change in area burned varied across scenarios. The 50th percentile was projected to increase (0.9–47.6 percent) for all scenarios. In contrast, the 95th percentile was projected to decrease under the A1B and B1 scenarios and increase under the A2 scenario. Under the ECHAM5 simulations, the 50th and 95th percentiles for the number of wildfires were projected to decrease across all scenarios (table 2.10, fig. 2.14*B*). General increases in the distribution of area burned were projected under the A1B and A2 scenarios, whereas decreases were projected under the B1 scenario. The simulation under the A1B scenario projected the largest change, with 44-percent and 17-percent increases projected for the 50th and 95th percentiles of area burned, respectively.

Table 2.10. Summary of fire activity for the Northwest Boreal Landscape Conservation Cooperative North simulated for the last decades of the historical period (2000–2009) and the projection period (2090–2099).

[The 50th (median) and 95th percentiles were computed across 200 model replicates for each future climate simulation. Details regarding the models and scenarios shown can be found in table 2.9. km², square kilometer]

Climate scenario	Metric (percentile)	Historical period		Projection period		Change in number of wildfires (percent)	Change in area burned (percent)
		Number of wildfires	Area burned (km²)	Number of wildfires	Area burned (km²)		
CGCM3.1							
A1B	Median	42	2,274	45	2,295	5.9	0.9
A1B	95th	62	10,342	64	10,199	3.5	–1.4
A2	Median	42	2,194	44	3,239	7.2	47.6
A2	95th	63	10,459	66	16,626	5.3	59.0
B1	Median	42	2,216	48	2,622	15.5	18.3
B1	95th	62	10,511	67	7,855	7.3	–25.3
ECHAM5							
A1B	Median	42	2,200	40	3,174	–3.6	44.3
A1B	95th	63	10,426	62	12,217	–0.6	17.2
A2	Median	42	2,186	37	2,176	–10.8	–0.5
A2	95th	63	10,422	61	12,642	–3.1	21.3
B1	Median	42	2,230	38	1,798	–7.2	–19.4
B1	95th	63	10,264	57	8,090	–9.2	–21.2

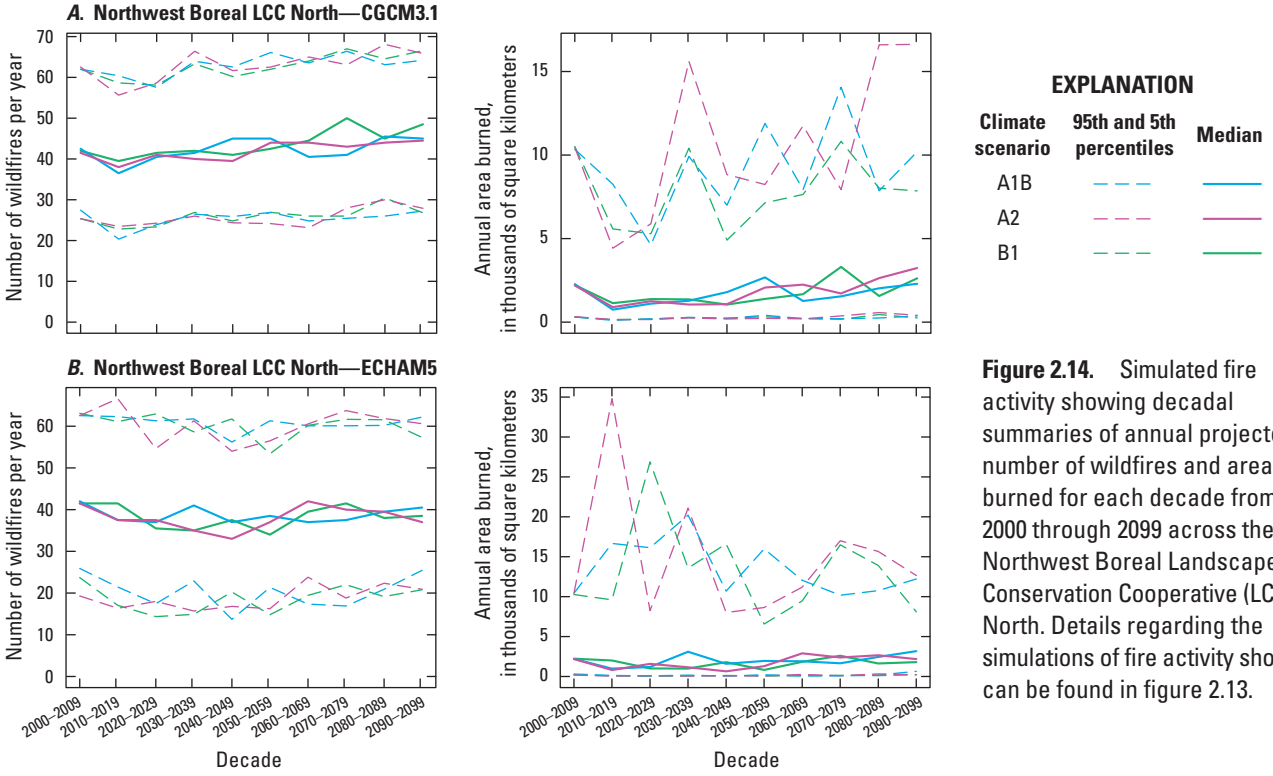

Figure 2.14. Simulated fire activity showing decadal summaries of annual projected number of wildfires and area burned for each decade from 2000 through 2099 across the Northwest Boreal Landscape Conservation Cooperative (LCC) North. Details regarding the simulations of fire activity shown can be found in figure 2.13.

The Western Alaska LCC had the second most historical fire activity among the five LCC regions and was also projected to have the second most future fire activity. Under the CGCM3.1 simulations, projected median changes in number of wildfires varied in magnitude and direction. Under the B1 and A2 scenarios, moderate increases were projected in the 50th percentile, whereas the greatest change among the scenarios was projected under the A1B scenario, with a decrease of 22.2 percent (table 2.11, fig. 2.15*A*). The distribution in area burned was projected to increase for all scenarios, except for the 50th percentile under the A1B scenario, which was projected to decrease. Under the B1 and A2 scenarios, large increases (139 percent and 180 percent, respectively) were projected in the 50th percentile. Under the ECHAM5 simulations, the 50th and 95th percentiles for the number of wildfires were projected to decrease across all scenarios (table 2.11, fig. 2.15*B*). The distribution of area burned was projected to increase under the A1B and A2 scenarios, whereas the 95th percentile under the B1 scenario was projected to decrease. The 50th percentile was projected to increase under each of the scenarios with the largest increases under the A2 and A1B scenarios (146 percent and 302 percent, respectively).

Table 2.11. Summary of fire activity for the Western Alaska Landscape Conservation Cooperative simulated for the last decades of the historical period (2000–2009) and the projection period (2090–2099).

[The 50th (median) and 95th percentiles were computed across 200 model replicates for each future climate simulation. Details regarding the models and scenarios shown can be found in table 2.9. km², square kilometer]

Climate scenario	Metric (percentile)	Historical period		Projection period		Change in number of wildfires (percent)	Change in area burned (percent)
		Number of wildfires	Area burned (km²)	Number of wildfires	Area burned (km²)		
CGCM3.1							
A1B	Median	9	714	7	344	–22.2	–51.8
A1B	95th	17	7,735	16	9,185	–7.9	18.8
A2	Median	8	332	8	929	6.2	179.8
A2	95th	17	7,315	16	10,729	–6.0	46.7
B1	Median	8	336	8	802	6.2	138.7
B1	95th	17	7,533	17	8,400	–2.6	11.5
ECHAM5							
A1B	Median	8	330	7	1,329	–17.6	302.7
A1B	95th	17	7,529	15	9,979	–14.4	32.5
A2	Median	8	334	7	824	–17.6	146.7
A2	95th	17	7,407	15	10,651	–12.1	43.8
B1	Median	8	332	6	360	–23.5	8.4
B1	95th	17	7,251	14	5,842	–18.1	–19.4

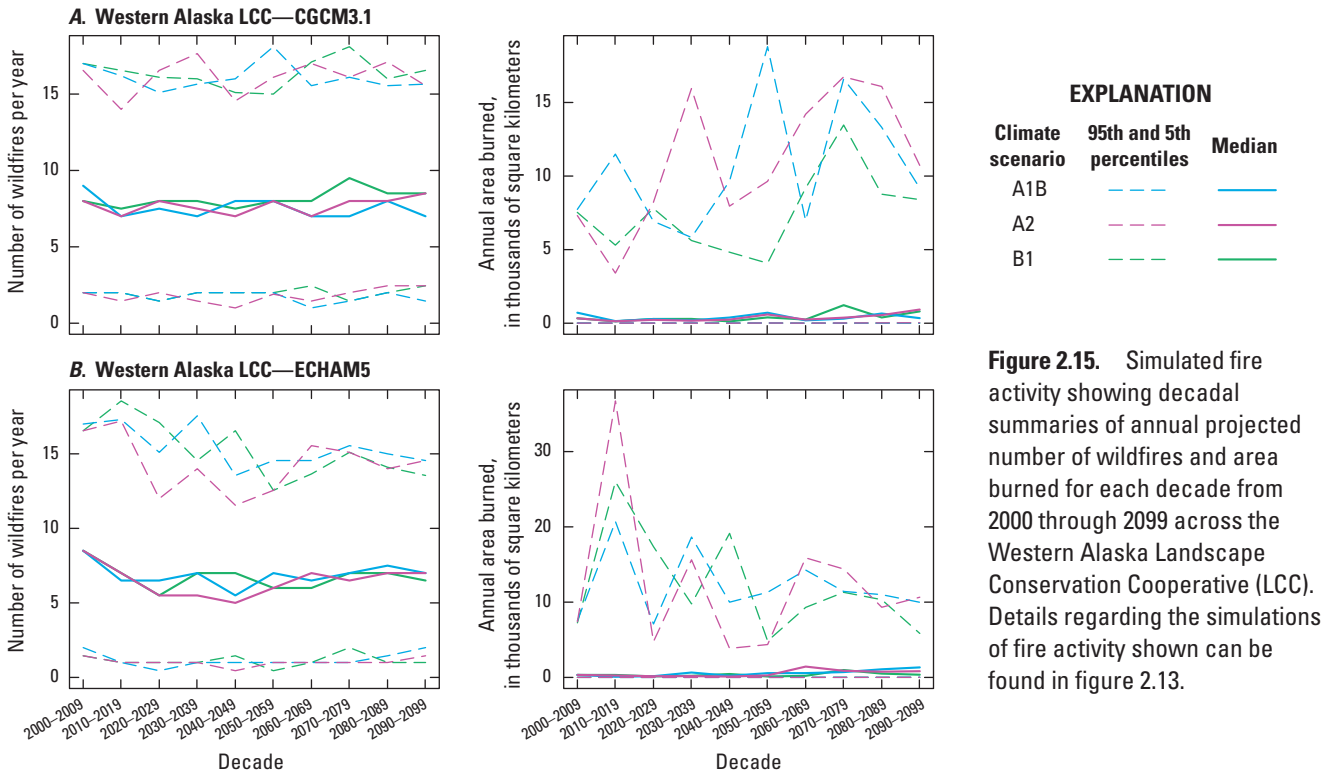

Figure 2.15. Simulated fire activity showing decadal summaries of annual projected number of wildfires and area burned for each decade from 2000 through 2099 across the Western Alaska Landscape Conservation Cooperative (LCC). Details regarding the simulations of fire activity shown can be found in figure 2.13.

In the Arctic LCC, no change was projected in the 50th percentile of the number of wildfires across all scenarios with CGCM3.1 (table 2.12, fig. 2.16*A*). The 95th percentile under the A1B and A2 scenarios was projected to increase. The projected change in area burned varied in magnitude and direction across scenarios. The 50th percentile was projected to increase under scenarios B1 and A2, whereas no change was projected under scenario A1B. The largest change was projected under the A2 scenario with an increase of 1,300 percent. The 95th percentile was projected to decrease under the B1 and A1B scenarios; however, the 95th percentile under the A2 scenario was projected to increase. Under the ECHAM5 simulations, the 50th percentile for the number of wildfires was not projected to change across all scenarios (table 2.12, fig. 2.16*B*). The 95th percentile under the B1 and A2 scenarios was projected to decrease, whereas that under the A1B scenario was projected to increase. The 50th percentile of the distribution of area burned was projected to increase across all of the scenarios, with the greatest (2,050-percent) increase projected under the A1B scenario. The 95th percentile was projected to decrease under the B1 and A2 scenarios, whereas an increase in the 95th percentile was projected under the A1B scenario.

Table 2.12. Summary of fire activity for the Arctic Landscape Conservation Cooperative simulated for the last decades of the historical period (2000–2009) and the projection period (2090–2099).

[The 50th (median) and 95th percentiles were computed across 200 model replicates for each future climate simulation. Details regarding the models and scenarios shown can be found in table 2.9. km², square kilometer]

Climate scenario	Metric (percentile)	Historical period		Projection period		Change in number of wildfires (percent)	Change in area burned (percent)
		Number of wildfires	Area burned (km²)	Number of wildfires	Area burned (km²)		
CGCM3.1							
A1B	Median	1	22	1	22	0	0
A1B	95th	3	5,553	4	4,128	18.3	–25.7
A2	Median	1	10	1	140	0	1,300
A2	95th	3	5,919	4	8,362	33.3	41.3
B1	Median	1	10	1	16	0	60
B1	95th	3	6,230	3	3,323	0	–46.7
ECHAM5							
A1B	Median	1	10	1	215	0	2,050
A1B	95th	3	6,058	4	7,525	18.3	24.2
A2	Median	1	10	1	56	0	460
A2	95th	3	6,042	3	5,473	–15	–9.4
B1	Median	1	10	1	40	0	300
B1	95th	4	6,232	3	1,421	–28.2	–77.2

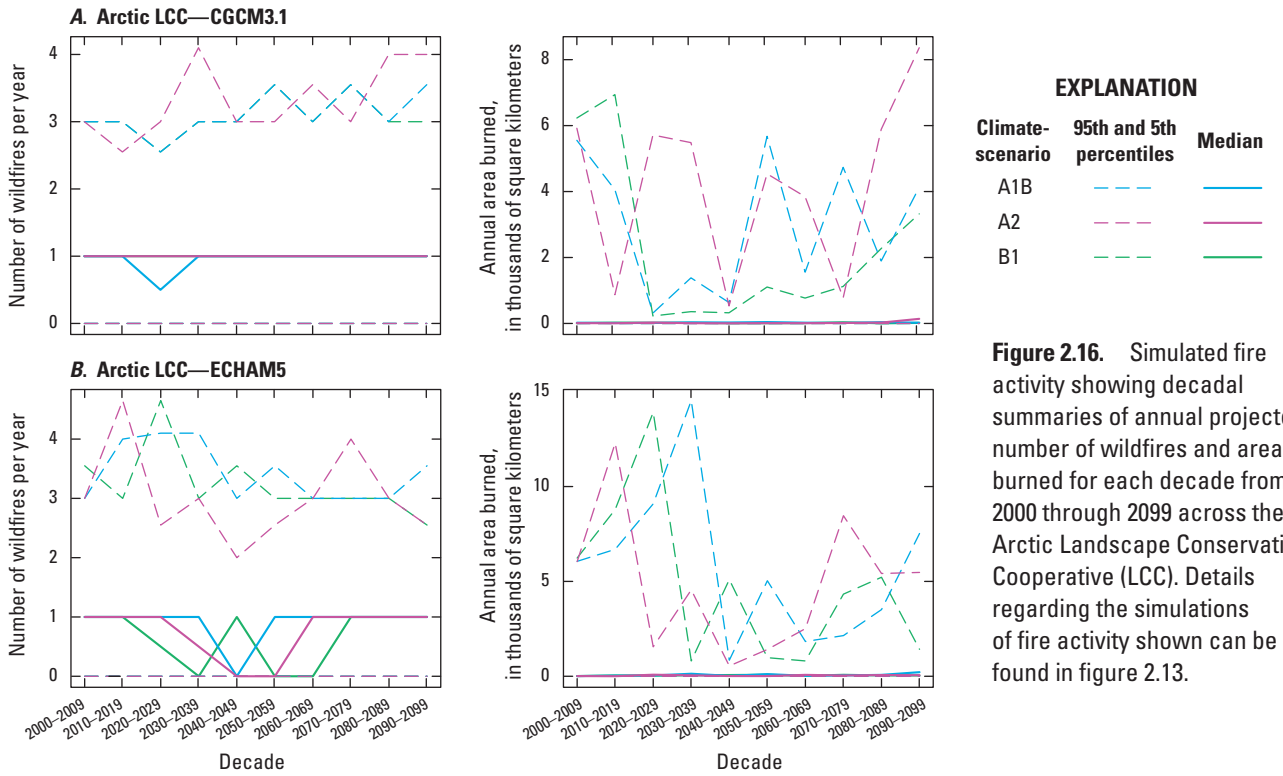

Figure 2.16. Simulated fire activity showing decadal summaries of annual projected number of wildfires and area burned for each decade from 2000 through 2099 across the Arctic Landscape Conservation Cooperative (LCC). Details regarding the simulations of fire activity shown can be found in figure 2.13.

In the Northwest Boreal LCC South, increases in the 50th and 95th percentiles for the number of wildfires were projected under the B1 and A2 scenarios with CGCM3.1, whereas decreases were projected under the A1B scenario (table 2.13, fig. 2.17*A*). The projected change in area burned varied in magnitude and direction across scenarios. The 50th percentile was projected to increase under the B1 and A2 scenarios. A decrease in the 95th percentile was projected under the B1 scenario, whereas an increase was projected under the A2 scenario. The magnitude of change was largest under the A2 scenario with the 50th percentile projected to increase by 107 percent and the 95th percentile projected to increase by 432 percent. Under the ECHAM5 simulations, the 50th and 95th percentiles for the number of wildfires were projected to decrease across all scenarios (table 2.13, fig. 2.17*B*). The 50th and 95th percentiles of the distribution of area burned were projected to increase under the A1B and A2 scenarios, whereas decreases were projected under the B1 scenario. The largest increase in the 50th percentile (51 percent) was projected under the A1B scenario, and the largest increase in the 95th percentile (110 percent) was projected under the A2 scenario.

Table 2.13. Summary of fire activity for the Northwest Boreal Landscape Conservation Cooperative South simulated for the last decades of the historical period (2000–2009) and the projection period (2090–2099).

[The 50th (median) and 95th percentiles were computed across 200 model replicates for each future climate simulation. Details regarding the models and scenarios shown can be found in table 2.9. km², square kilometer]

Climate scenario	Metric (percentile)	Historical period		Projection period		Change in number of wildfires (percent)	Change in area burned (percent)
		Number of wildfires	Area burned (km²)	Number of wildfires	Area burned (km²)		
CGCM3.1							
A1B	Median	10	264	10	167	–5	–36.7
A1B	95th	20	2,337	18	1,355	–7.9	–42.0
A2	Median	10	208	10	430	10.5	106.7
A2	95th	20	2,355	22	12,523	10.2	431.8
B1	Median	10	204	11	258	15.8	26.5
B1	95th	20	2,328	20	2,064	2.3	–11.3
ECHAM5							
A1B	Median	10	203	9	308	–5.3	51.7
A1B	95th	20	2,362	19	8,689	–2.3	267.9
A2	Median	10	200	8	203	–15.8	1.5
A2	95th	20	2,289	18	4,810	–10.2	110.1
B1	Median	10	212	8	143	–10.5	–32.5
B1	95th	20	2,283	17	1,298	–15.3	–43.1

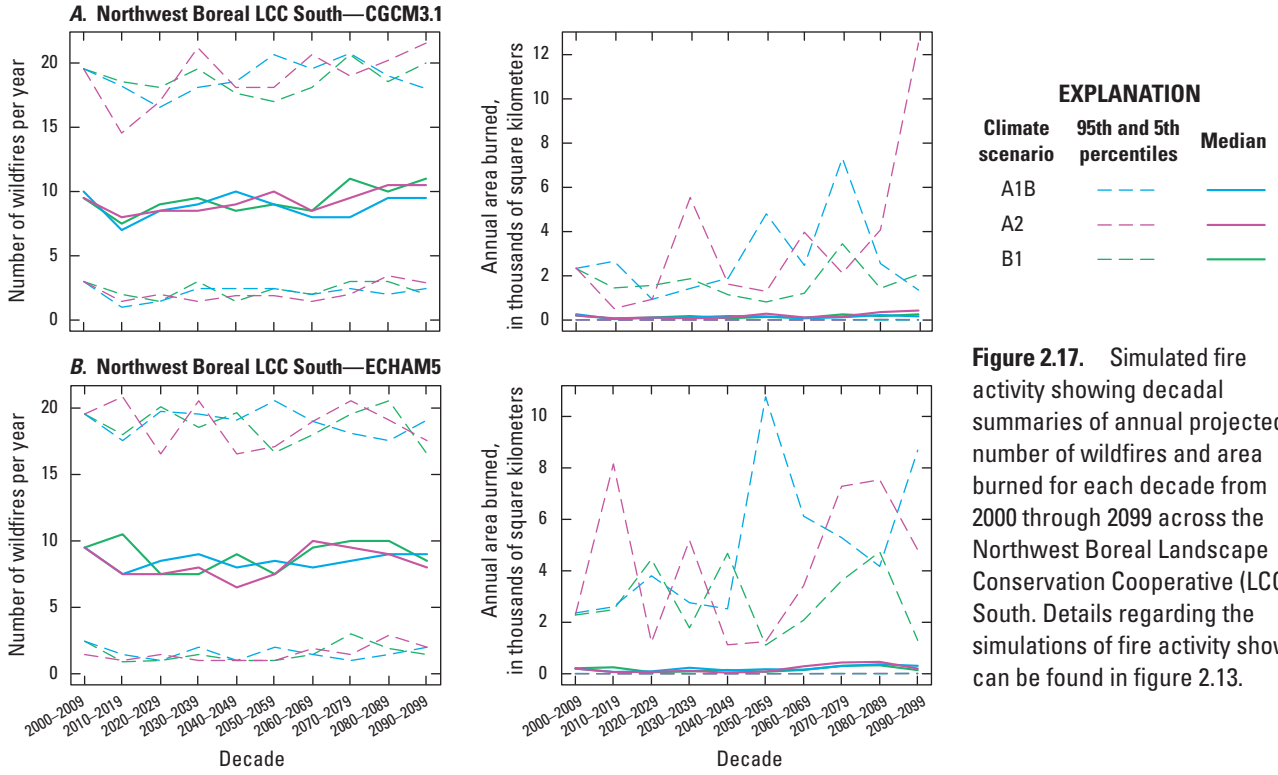

Figure 2.17. Simulated fire activity showing decadal summaries of annual projected number of wildfires and area burned for each decade from 2000 through 2099 across the Northwest Boreal Landscape Conservation Cooperative (LCC) South. Details regarding the simulations of fire activity shown can be found in figure 2.13.

Of the five assessment regions, the North Pacific LCC had the least amount of fire activity reflecting the LCC's wet and cool climate. Future simulations showed little indication of any meaningful future fire activity in this region (table 2.14, fig. 2.18*A*, *B*).

Table 2.14. Summary of fire activity for the North Pacific Landscape Conservation Cooperative simulated for the last decades of the historical period (2000–2009) and the projection period (2090–2099).

[The 50th (median) and 95th percentiles were computed across 200 model replicates for each future climate simulation. Details regarding the models and scenarios shown can be found in table 2.9. km², square kilometer; —, not applicable]

Climate scenario	Metric (percentile)	Historical period		Projection period		Change in number of wildfires (percent)	Change in area burned (percent)
		Number of wildfires	Area burned (km²)	Number of wildfires	Area burned (km²)		
CGCM3.1							
A1B	Median	0	2	0	2	—	—
A1B	95th	2	27	2	28	–22.5	3.7
A2	Median	0	2	0	5	—	—
A2	95th	2	25	3	160	64.52	540
B1	Median	0	2	0	2	—	—
B1	95th	2	25	2	25	0	0
ECHAM5							
A1B	Median	0	2	0	6	—	—
A1B	95th	2	25	3	274	93.55	996
A2	Median	0	2	0	4	—	—
A2	95th	2	24	3	121	64.52	404.17
B1	Median	0	2	0	2	—	—
B1	95th	2	23	2	44	29.03	91.3

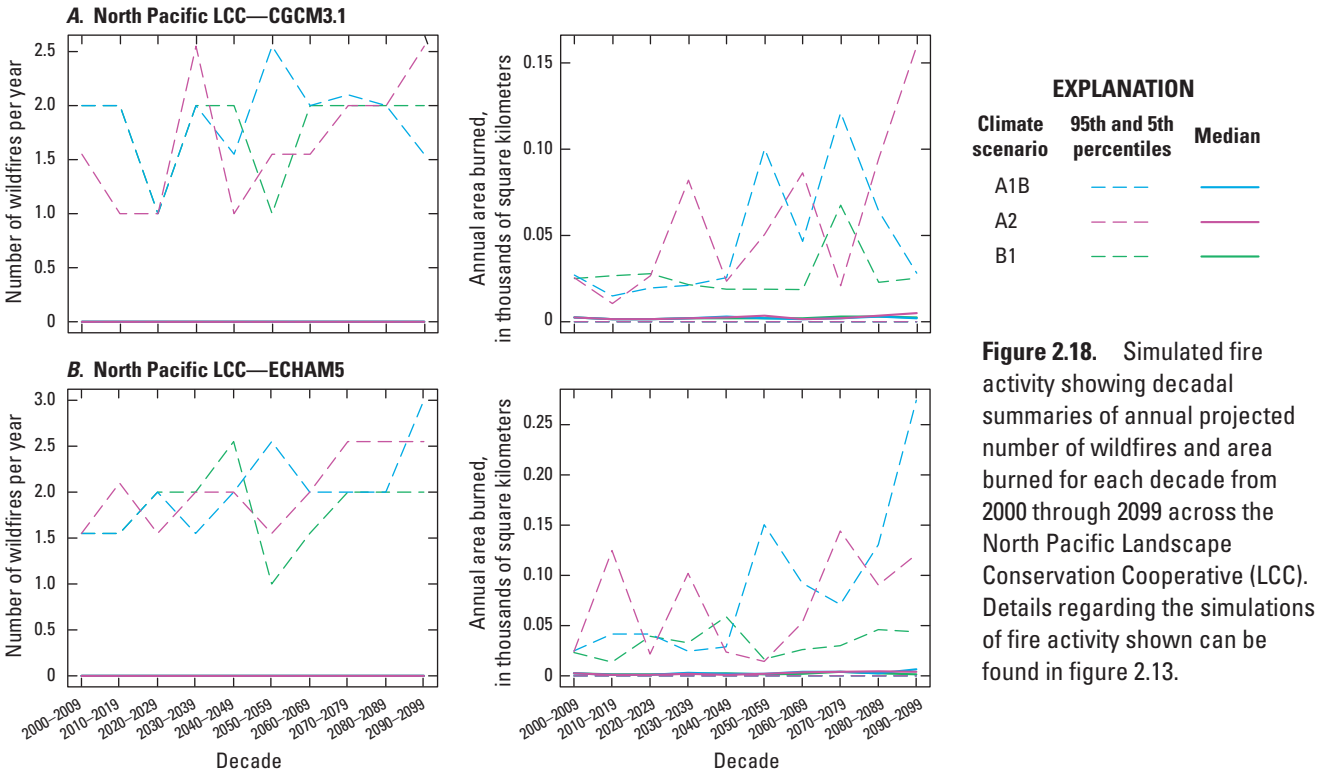

Figure 2.18. Simulated fire activity showing decadal summaries of annual projected number of wildfires and area burned for each decade from 2000 through 2099 across the North Pacific Landscape Conservation Cooperative (LCC). Details regarding the simulations of fire activity shown can be found in figure 2.13.

2.4.6. Discussion and Conclusions

Climate effects, both direct and indirect, are projected to influence the vegetation-disturbance dynamics of Alaska through the 21st century. Most of the vegetation change simulated by ALFRESCO would result from the indirect effects of climate as mediated by the fire regime. On the basis of the characterization of fire-climate relationships from the past six decades, fire regimes are forecast to change for most of the simulations considered. The Northwest Boreal LCC North would exhibit the greatest amount of change in simulated fire activity relative to historical observations. One of the dominant results following from this projected change in fire regimes is a projected decrease in the area occupied by late successional spruce forests. This decrease would be consistent across all the climate simulations for Alaska as a whole and in most of the five LCC regions.

One of the defining characteristics of the fire regime in Alaska is significant variability across both space and time. The simulated fire activity from both GCMs produced large inter-annual variability in the fire activity in a manner consistent with the historical fire data in Alaska. A steady increase in both the number of wildfires and median area burned after 2050 was projected for CGCM3.1 simulations under all scenarios. The variability of the distribution of simulated area burned also was projected to increase, as depicted by the increase in the 95th percentiles across the second half of the 21st century. In contrast, under the ECHAM5 simulations across all scenarios a small decrease in the number of wildfires and an increase in the median area burned after 2050 were projected as well as a decrease in the variability of the distribution of simulated area burned, shown in the 95th percentile.

The differences between the CGCM3.1 and ECHAM5 simulation output for the period 2010–2030 is driven largely by changes in the climate forcing of the fire activity. This is a consequence of the fact that the initial spatial distribution of differentially flammable vegetation is relatively consistent among simulations since it is determined by the patterns of historical fire. As the changes in future climate affect the landscape configuration of vegetation types through fire-initiated secondary succession, there are potential feedbacks to the fire regime. This is likely the reason that there are differences in the trends of the number of wildfires between the GCMs. That is, differences in the spatial configuration of differentially flammable vegetation types emerge uniquely for the GCMs as a function of the climate forcing effects on the fire regime. Ultimately, the configuration of the landscape dictates how the fire activity emerges for the climate signal in each year.

Simulated land-cover types in tundra-dominated portions of the assessment domain exhibited moderate levels of change. Graminoid tundra was projected to decrease under most of the future climate simulations, whereas shrub tundra was projected to increase. The magnitude and direction of change would vary considerably across the LCC regions, though consistently within each region. That is, in the Arctic LCC, graminoid tundra was projected to decrease and shrub tundra was projected to increase across the simulations, whereas opposite trends were projected for the Western Alaska LCC. These patterns reflect positive influences of a warming climate, in the case of shrub tundra increases in the Arctic LCC, as well as the indirect effects through wildfire activity, in the case of shrub tundra decreases in the Western Alaska LCC.

2.4.6.1. Uncertainty

The use of models to simulate future fire activity provides a means to assemble the state of the science and assess the likely responses to future scenarios. Generally speaking, models are developed with the intent to characterize the functional relationships between ecological responses and environmental drivers. One metric of model performance is to meaningfully explain the observed variability in an ecological response at varying resolutions of space and time. Best performing models are able to parsimoniously explain variability in a manner that is robust to the multiple sources of uncertainty that are constrained through assumptions.

The projections presented here were generated through the development of several layers of modeling, each with its own corresponding uncertainty. The process starts with data. One can consider data to be an observation of some underlying true latent process. In most settings, observed data are considered to be truth. That is, the difference between the observed value and the true state of the underlying latent process is zero. This is the implementation of the time-honored uncertainty reduction technique of assumption making. In some cases this is appropriate, in others it may make more sense to employ a hierarchical modeling approach to separate the uncertainty associated with the input data from that of the process model (Calder and others, 2003; Cressie and Wikle, 2011). When constructing simulation models, whether statistical, process-based, or otherwise, there is uncertainty associated with the functional form of the model. Finally, there is uncertainty associated with the parameters that are estimated in the modeling process.

In the work presented here, we explicitly considered uncertainty in the simulations of future fire activity that is associated with the GCMs and emissions scenarios. This was done by running simulations for different combinations of GCMs and scenarios. Bounding results were presented in the sense that the ECHAM5 model generally corresponds to the most active future fire regime and the CGCM3.1 model to the least. In using this approach, we conditioned on the functional relationship depicted in the ALFRESCO model and assumed this was the best model through the application of calibration to the historical data. That is, uncertainty in the depiction of the functional linkage between future climate and fire was constrained. One potential source of uncertainty associated with the results is the potential for the functional linkage between climate and fire to change in the future.

The historical data were also assumed, for the sake of these analyses, to be unbiased representations of the true underlying latent process of fire across the boreal forest. This assumption was used when quantifying the linkage between climate and area burned based on the historical data. There is good reason to think this is not the case in Alaska and, understandably, the reliability of the historical fire data is more questionable for the earlier part of the record (Kasischke and others, 2002, 2006). To some extent, issues related to the uncertainty associated with the data are potentially reduced owing to the increased detectability associated with large fire events. That is, it is more likely to miss a smaller fire in the record than a larger one. Since over half of the area burned in Alaska comes from approximately the largest 2.5 percent of the fires (Kasischke and Turetsky, 2006), these issues associated with uncertainty in the data are likely negligible relative to the uncertainty associated with the actual unfolding of the future climate scenario.

When considering the full assessment domain, the uncertainty associated with the projected results was greater between GCMs than it was between the emissions scenarios for a given GCM, which tend to be generally consistent. This assertion holds less credence when considering the LCC regions. To some extent this may be driven by the simple fact that there was greater variability among replicates for the consideration of smaller landscape areas.

2.4.6.2. Sensitivity

When considering the greatest potential for change in the future scenarios, it is of interest to examine not only the measure of central tendency for the future scenarios but also higher statistical moments as well. Across the entire State, there were divergent results among GCMs with respect to the change in number of wildfires. The 50th and 95th percentiles of the wildfire distributions were projected to increase for all scenarios in the CGCM3.1 model, whereas the corresponding simulated data were projected to decrease in the ECHAM5 model. Projected ignitions were placed in a spatially random manner so an increase would correspond to increases in the temperature and (or) prevalence of flammable vegetation across the landscape. The increase in number of wildfires suggests the potential for a subsequent increase in the heterogeneity of the landscape as a consequence. Across the entire State, the simulation output projected an increase in the area burned with more burning associated with the CGCM3.1 model. Interestingly, along with the increase in area burned was an opposite response in the change through time between the 95th percentiles of the CGCM3.1 and the ECHAM5 models. The CGCM3.1 model projected an increase in number of wildfires and an increase in the variability of area burned, whereas the ECHAM5 model projected a relatively stable number of wildfires and a steady decrease in the variability of area burned through time. In this context, the CGCM3.1 model projects a much more variable future with respect to landscape-scale disturbance.

When considering the LCC regions, several stand out as being most sensitive in terms of future changes in the fire regime. The North Pacific LCC had the lowest historical fire activity so any future increase would be a relatively large shift, although the absolute amount of fire activity may be negligible in the context of statewide area burned. The variability of the number of wildfires and the variability associated with the distribution of the simulated area burned were projected to increase consistently over the projection period in the North Pacific LCC. In this sense, the simulated results are consistent among all simulations, projecting that there would be a relatively large increase in fire activity. This is an example of a region where there appears to be potential for a threshold to be crossed (that is, for greater influence of fire activity) in the next century.

The simulation results also indicate that the Northwest Boreal LCC South may experience increased wildfires and area burned in the future. The ECHAM5 model projected a relatively constant number of wildfires but an increase in the variability of the area burned under the A2 and A1B scenarios. The CGCM3.1 model projected an increase in number of wildfires, but only under the A2 scenario was a corresponding increase in the variability of the area burned projected.

The simulation results for the Western Alaska LCC were relatively divergent between the two GCMs. For the CGCM3.1 model, the number of wildfires forecast was relatively constant; however, a forecast increase in the variability of area burned was consistent across the scenarios considered. Conversely, for the ECHAM5 model, the number of wildfires was projected to decrease with a corresponding decrease in the variability associated with the distribution of area burned. Thus, the sensitivity of the Western Alaska LCC to changes in future climate over the 21st century is dependent on the model used to simulate the future climate, with the CGCM3.1 model being more sensitive and the ECHAM5 model relatively stable and therefore less sensitive to climate change.

2.5. References Cited

Amiro, B.D., Todd, J.B., Wotton, B.M., Logan, K.A., Flannigan, M.D., Stocks, B.J., Mason, J.A., Martell, D.L., and Hirsch, K.G., 2001, Direct carbon emissions from Canadian forest fires, 1959–1999: Canadian Journal of Forest Research, v. 31, no. 3, p. 512–525, http://dx.doi.org/10.1139/x00-197.

Balshi, M.S., McGuire, A.D., Duffy, Paul, Flannigan, Mike, Walsh, John, and Melillo, Jerry, 2009, Assessing the response of area burned to changing climate in western boreal North America using a Multivariate Adaptive Regression Splines (MARS) approach: Global Change Biology, v. 15, no. 3, p. 578–600, http://dx.doi.org/10.1111/j.1365-2486.2008.01679.x.

Barber, V.A., Juday, G.P., and Finney, B.P., 2000, Reduced growth of Alaskan white spruce in the twentieth century from temperature-induced drought stress: Nature, v. 405, no. 6787, p. 668–673, http://dx.doi.org/10.1038/35015049.

Barber, V.A., Juday, G.P., Finney, B.P., and Wilmking, Martin, 2004, Reconstruction of summer temperatures in interior Alaska from tree-ring proxies; Evidence for changing synoptic climate regimes: Climatic Change, v. 63, nos. 1–2, p. 91–120, http://dx.doi.org/10.1023/B:CLIM.0000018501.98266.55.

Beck, P.S.A., Juday, G.P., Alix, Claire, Barber, V.A., Winslow, S.E., Sousa, E.E., Heiser, Patricia, Herriges, J.D., and Goetz, S.J., 2011, Changes in forest productivity across Alaska consistent with biome shift: Ecology Letters, v. 14, no. 4, p. 373–379, http://dx.doi.org/10.1111/j.1461-0248.2011.01598.x.

Berg, E.E., Hillman, K.M., Dial, Roman, and DeRuwe, Allana, 2009, Recent woody invasion of wetlands on the Kenai Peninsula Lowlands, south-central Alaska; A major regime shift after 18,000 years of wet *Sphagnum*-sedge peat recruitment: Canadian Journal of Forest Research, v. 39, no. 11, p. 2033–2046, http://dx.doi.org/10.1139/X09-121.

Burn, C.R., Mackay, J.R., and Kokelj, S.V., 2009, The thermal regime of permafrost and its susceptibility to degradation in upland terrain near Inuvik, N.W.T.: Permafrost and Periglacial Processes, v. 20, no. 2, p. 221–227, http://dx.doi.org/10.1002/ppp.649.

Calder, Catherine, Lavine, Michael, Müller, Peter, and Clark, J.S., 2003, Incorporating multiple sources of stochasticity into dynamic population models: Ecology, v. 84, no. 6, p. 1395–1402, http://dx.doi.org/10.1890/0012-9658(2003)084[1395:IMSOSI]2.0.CO;2.

Chapman, W.L., and Walsh, J.E., 1993, Recent variations of sea ice and air temperature in high latitudes: Bulletin of the American Meteorological Society, v. 74, no. 1, p. 33–47, http://dx.doi.org/10.1175/1520-0477(1993)074<0033:RVOSIA>2.0.CO;2.

Cressie, Noel, and Wikle, C.K., 2011, Statistics for spatio-temporal data: Hoboken, N.J., John Wiley & Sons, Inc., 588 p.

Daly, Christopher, Halbleib, Michael, Smith, J.I., Gibson, W.P., Doggett, M.K., Taylor, G.H., Curtis, Jan, and Pasteris, P.P., 2008, Physiographically sensitive mapping of climatological temperature and precipitation across the conterminous United States: International Journal of Climatology, v. 28, no. 15, p. 2031–2064, http://dx.doi.org/10.1002/joc.1688.

Duffy, P.A., Epting, Justin, Graham, J.M., Rupp, T.S., and McGuire, A.D., 2007, Analysis of Alaskan burn severity patterns using remotely sensed data: International Journal of Wildland Fire, v. 16, no. 3, p. 277–284, http://dx.doi.org/10.1071/WF06034.

Duffy, P.A., Walsh, J.E., Graham, J.M., Mann, D.H., and Rupp, T.S., 2005, Impacts of large-scale atmospheric-ocean variability on Alaskan fire season severity: Ecological Applications, v. 15, no. 4, p. 1317–1330, http://dx.doi.org/10.1890/04-0739.

Dyrness, C.T., and Norum, R.A., 1983, The effects of experimental fires on black spruce forest floors in interior Alaska: Canadian Journal of Forest Research, v. 13, no. 5, p. 879–893, http://dx.doi.org/10.1139/x83-118.

Euskirchen, E.S., McGuire, A.D., Rupp, T.S., Chapin, F.S., III, and Walsh, J.E., 2009, Projected changes in atmospheric heating due to changes in fire disturbance and the snow season in the western Arctic, 2003–2100: Journal of Geophysical Research; Biogeosciences, v. 114, no. G4, article G04022, 15 p., http://dx.doi.org/10.1029/2009JG001095.

Flato, G.M., 2005, The third generation Coupled Global Climate Model (CGCM3) [and included links to the description of the AGCM3 atmospheric model]: Canadian Centre for Climate Modelling and Analysis, accessed September 1, 2014, at http://ec.gc.ca/ccmac-cccma/default.asp?lang=En&n=1299529F-1.

Genet, H., McGuire, A.D., Barrett, K., Breen, A., Euskirchen, E.S., Johnstone, J.F., Kasischke, E.S., Melvin, A.M., Bennett, A., Mack, M.C., Rupp, T.S., Schuur, E.A.G., Turetsky, M.R., and Yuan, F., 2013, Modeling the effects of fire severity and climate warming on active layer thickness and soil carbon storage of black spruce forests across the landscape in interior Alaska: Environmental Research Letters, v. 8, no. 4, letter 045016, 13 p., http://dx.doi.org/10.1088/1748-9326/8/4/045016.

Gillett, N.P., Weaver, A.J., Zwiers, F.W., and Flannigan, M.D., 2004, Detecting the effect of climate change on Canadian forest fires: Geophysical Research Letters, v. 31, no. 18, letter L18211, 4 p., http://dx.doi.org/10.1029/2004GL020876.

Goetz, S.J., Bunn, A.G., Fiske, G.J., and Houghton, R.A., 2005, Satellite-observed photosynthetic trends across boreal North America associated with climate and fire disturbance: National Academy of Sciences Proceedings, v. 102, no. 38, p. 13521–13525, http://dx.doi.org/10.1073/pnas.0506179102.

Gustine, D.D., Brinkman, T.J., Lindgren, M.A., Schmidt, J.I., Rupp, T.S., and Adams, L.G., 2014, Climate-driven effects of fire on winter habitat for caribou in the Alaskan-Yukon Arctic: PLOS ONE, v. 9, no. 7, article e100588, 11 p., http://dx.doi.org/10.1371/journal.pone.0100588.

Harris, I., Jones, P.D., Osborn, T.J., and Lister, D.H., 2014, Updated high-resolution grids of monthly climatic observations—the CRU TS3.10 dataset: International Journal of Climatology, v. 34, no. 3, p. 623–642, http://dx.doi.org/10.1002/joc.3711.

Hartmann, Brian, and Wendler, Gerd, 2005, The significance of the 1976 Pacific climate shift in the climatology of Alaska: Journal of Climate, v. 18, no. 22, p. 4824–4839, http://dx.doi.org/10.1175/JCLI3532.1.

Hay, L.E., Wilby, R.L., and Leavesley, G.H., 2000, A comparison of delta change and downscaled GCM scenarios for three mountainous basins in the United States: Journal of the American Water Resources Association, v. 36, no. 2, p. 387–397, http://dx.doi.org/10.1111/j.1752-1688.2000.tb04276.x.

Hayes, D.J., McGuire, A.D., Kicklighter, D.W., Gurney, K.R., Burnside, T.J., and Melillo, J.M., 2011, Is the northern high-latitude land-based CO_2 sink weakening?: Global Biogeochemical Cycles, v. 25, no. 3, article GB3018, 14 p., http://dx.doi.org/10.1029/2010GB003813.

Hayhoe, K.A., 2010, A standardized framework for evaluating the skill of regional climate downscaling techniques: Urbana-Champaign, Ill., University of Illinois, Ph.D. dissertation, 153 p. [Also available at http://hdl.handle.net/2142/16044.]

Hennon, P., D'Amore, D., Wittwer, D., Johnson, A., Schaberg, P., Hawley, G., Beier, C., Sink, S., and Juday, G., 2006, Climate warming, reduced snow, and freezing injury could explain the demise of yellow-cedar in southeast Alaska, USA: World Resource Review, v. 18, no. 2, p. 427–450. [Also available at http://www.fs.usda.gov/Internet/FSE_DOCUMENTS/fsbdev2_038021.pdf.]

Hinzman L.D., Bettez, N.D., Bolton, W.R., Chapin, F.S., Dyurgerov, M.B., Fastie, C.L., Griffith, Brad, Hollister, R.D., Hope, Allen, Huntington, H.P., Jensen, A.M., Jia, G.J., Jorgenson, Torre, Kane, D.L., Klein, D.R., Kofinas, Gary, Lynch, A.H., Lloyd, A.H., McGuire, A.D., Nelson, F.E., Oechel, W.C., Osterkamp, T.E., Racine, C.H., Romanovsky, V.E., Stone, R.S., Stow, D.A., Sturm, Matthew, Tweedie, C.E., Vourlitis, G.L., Walker, M.D., Walker, D.A., Webber, P.J., Welker, J.M., Winker, K.S., and Yoshikawa, Kenji, 2005, Evidence and implications of recent climate change in northern Alaska and other arctic regions: Climatic Change, v. 72, no. 3, p. 251–298, http://dx.doi.org/10.1007/s10584-005-5352-2.

Johnstone, J.F., Chapin, F.S., III, Hollingsworth, T.N., Mack, M.C., Romanovsky, Vladimir, and Turetsky, Merritt, 2010, Fire, climate change, and forest resilience in interior Alaska: Canadian Journal of Forest Research, v. 40, no. 7, p. 1302–1312, http://dx.doi.org/10.1139/X10-061.

Johnstone, J.F., Rupp, T.S., Olson, Mark, and Verbyla, David, 2011, Modeling impacts of fire severity on successional trajectories and future fire behavior in Alaskan boreal forests: Landscape Ecology, v. 26, no. 4, p. 487–500, http://dx.doi.org/10.1007/s10980-011-9574-6.

Jorgenson, M.T., Racine, C.H., Walters, J.C., and Osterkamp, T.E., 2001, Permafrost degradation and ecological changes associated with a warming climate in central Alaska: Climatic Change, v. 48, no. 4, p. 551–579, http://dx.doi.org/10.1023/A:1005667424292.

Kasischke, E.S., Hyer, E.J., Novelli, P.C., Bruhwiler, L.P., French, N.H.F., Sukhinin, A.I., Hewson, J.H., and Stocks, B.J., 2005, Influences of boreal fire emissions on Northern Hemisphere atmospheric carbon and carbon monoxide: Global Biogeochemical Cycles, v. 19, no. 1, article GB1012, 16 p., http://dx.doi.org/10.1029/2004GB002300.

Kasischke, E.S., O'Neill, K.P., French, N.H.F., and Bourgeau-Chavez, L.L., 2000, Controls on patterns of biomass burning in Alaskan boreal forests, chap. 10 *of* Kasischke, E.S., and Stocks, B.J., eds., Fire, climate change, and carbon cycling in the boreal forest: New York, Springer-Verlag, Ecological Studies, v. 138, p. 173–196.

Kasischke, E.S., Rupp, T.S., and Verbyla, D.L., 2006, Fire trends in the Alaskan boreal forest, chap. 17 *of* Chapin, F.S., III, Oswood, M.W., Van Cleve, Keith, Viereck, L.A., and Verbyla, D.L., eds., Alaska's changing boreal forest: New York, Oxford University Press, p. 285–301.

Kasischke, E.S., and Turetsky, M.R., 2006, Recent changes in the fire regime across the North American boreal region—Spatial and temporal patterns of burning across Canada and Alaska: Geophysical Research Letters, v. 33, no. 9, letter L09703, 5 p., http://dx.doi.org/10.1029/2006GL025677.

Kasischke, E.S., Verbyla, D.L., Rupp, T.S., McGuire, A.D., Murphy, K.A., Jandt, Randi, Barnes, J.L., Hoy, E.E., Duffy, P.A., Calef, Monika, and Turetsky, M.R., 2010, Alaska's changing fire regime—Implications for the vulnerability of its boreal forests: Canadian Journal of Forest Research, v. 40, no. 7, p. 1313–1324, http://dx.doi.org/10.1139/X10-098.

Kasischke, E.S., Williams, David, and Barry, Donald, 2002, Analysis of the patterns of large fires in the boreal forest region of Alaska: International Journal of Wildland Fire, v. 11, no. 2, p. 131–144, http://dx.doi.org/10.1071/WF02023.

Kaufman, D.S., Schneider, D.P., McKay, N.P., Ammann, C.M., Bradley, R.S., Briffa, K.R., Miller, G.H., Otto-Bliesner, B.L., Overpeck, J.T., Vinther, B.M., and Arctic Lakes 2k Project Members, 2009, Recent warming reverses long-term Arctic cooling: Science, v. 325, no. 5945, p. 1236–1239, http://dx.doi.org/10.1126/science.1173983.

Kharuk, V.I., Dvinskaya, M.L., and Ranson, K.J., 2013, Fire return intervals within the northern boundary of the larch forest in central Siberia: International Journal of Wildland Fire, v. 22, no. 2, p. 207–211, http://dx.doi.org/10.1071/WF11181.

Mann, D.H., Rupp, T.S., Olson, M.A., and Duffy, P.A., 2012, Is Alaska's boreal forest now crossing a major ecological threshold?: Arctic, Antarctic, and Alpine Research, v. 44, no. 3, p. 319–331, http://dx.doi.org/10.1657/1938-4246-44.3.319.

Mantua, N.J., Hare, S.R., Zhang, Yuan, Wallace, J.M., and Francis, R.C., 1997, A Pacific interdecadal climate oscillation with impacts on salmon production: Bulletin of the American Meteorological Society, v. 78, no. 6, p. 1069–1079, http://dx.doi.org/10.1175/1520-0477(1997)078<1069:APICOW>2.0.CO;2.

Markon, C.J., Trainor, S.F., and Chapin, F.S., III, eds., 2012, The United States National Climate Assessment—Alaska Technical Regional Report: U.S. Geological Survey Circular 1379, 148 p. [Also available at http://pubs.usgs.gov/circ/1379/.]

McFarlane, N.A., Boer, G.J., Blanchet, J.-P., and Lazare, M., 1992, The Canadian Climate Centre second-generation general circulation model and its equilibrium climate: Journal of Climate, v. 5, no. 10, p. 1013–1044, http://dx.doi.org/10.1175/1520-0442(1992)005<1013:TCCCSG>2.0.CO;2.

McGuire, A.D., Ruess, R.W., Lloyd, A., Yarie, J., Clein, J.S., and Juday, G.P., 2010, Vulnerability of white spruce tree growth in interior Alaska in response to climate variability; Dendrochronological, demographic, and experimental perspectives: Canadian Journal of Forest Research, v. 40, no. 7, p. 1197–1209, http://dx.doi.org/10.1139/X09-206.

Meehl, G.A., Covey, Curt, Taylor, K.E., Delworth, Thomas, Stouffer, R.J., Latif, Mojib, McAvaney, Bryant, and Mitchell, J.F.B., 2007, The WCRP CMIP3 multimodel dataset—A new era in climate change research: Bulletin of the American Meteorological Society, v. 88, no. 9, p. 1383–1394, http://dx.doi.org/10.1175/BAMS-88-9-1383.

Myers-Smith, I.H., Harden, J.W., Wilmking, M., Fuller, C.C., McGuire, A.D., and Chapin, F.S., III, 2008, Wetland succession in a permafrost collapse; Interactions between fire and thermokarst: Biogeosciences, v. 5, no. 5, p. 1273–1286, http://dx.doi.org/10.5194/bg-5-1273-2008.

Nakićenović, Nebojša, and Swart, Robert, eds., 2000, Special report on emissions scenarios—A special report of Working Group III of the Intergovernmental Panel on Climate Change: Cambridge, United Kingdom, Cambridge University Press, 599 p. [Also available at http://www.ipcc.ch/ipccreports/sres/emission/index.php?idp=0.]

North American Land Change Monitoring System, 2010, 2005 North American land cover at 250 m spatial resolution (edition 1.0): Natural Resources Canada/Canadian Center for Remote Sensing (NRCan/CCRS), United States Geological Survey (USGS); Insituto Nacional de Estadística y Geografía (INEGI), Comisión Nacional para el Conocimiento y Uso de la Biodiversidad (CONABIO), and Comisión Nacional Forestal (CONAFOR), accessed October 30, 2011, at http://www.cec.org/tools-and-resources/map-files/land-cover-2005.

Overland, J.E., Spillane, M.C., Percival, D.B., Wang, Muyin, and Mofjeld, H.O., 2004, Seasonal and regional variation of pan-Arctic surface air temperature over the instrumental record: Journal of Climate, v. 17, no. 17, p. 3263–3282, http://dx.doi.org/10.1175/1520-0442(2004)017<3263:SARVOP>2.0.CO;2.

Overpeck, J., Hughen, K., Hardy, D., Bradley, R., Case, R., Douglas, M., Finney, B., Gajewski, K., Jacoby, G., Jennings, A., Lamoureux, S., Lasca, A., MacDonald, G., Moore, J., Retelle, M., Smith, S., Wolfe, A., and Zielinski, G., 1997, Arctic environmental change of the last four centuries: Science, v. 278, no. 5341, p. 1251–1256, http://dx.doi.org/10.1126/science.278.5341.1251.

Randerson, J.T., Liu, H., Flanner, M.G., Chambers, S.D., Jin, Y., Hess, P.G., Pfister, G., Mack, M.C., Treseder, K.K., Welp, L.R., Chapin, F.S., Harden, J.W., Goulden, M.L., Lyons, E., Neff, J.C., Schurr, E.A.G., and Zender, C.S., 2006, The impact of boreal forest fire on climate warming: Science, v. 314, no. 5802, p. 1130–1132, http://dx.doi.org/10.1126/science.1132075.

Roeckner, E., Bäuml, G., Bonaventura, L., Brokopf, R., Esch, M., Giorgetta, M., Hagemann, S., Kirchner, I., Kornblueh, L., Manzini, E., Rhodin, A., Schlese, U., Schulzweida, U., and Tompkins, A., 2003, The atmospheric general circulation model ECHAM5, part I—Model description: Max-Planck-Institut für Meteorologie Report, no. 349, 127 p. [Also available at https://www.mpimet.mpg.de/fileadmin/publikationen/Reports/max_scirep_349.pdf.]

Roeckner, E., Brokopf, R., Esch, M., Giorgetta, M., Hagemann, S., Kornblueh, L., Manzini, E., Schlese, U., and Schulzweida, U., 2004, The atmospheric general circulation model ECHAM5, part II—Sensitivity of simulated climate to horizontal and vertical resolution: Max-Planck-Institut für Meteorologie Report, no. 354, 56 p. [Also available at http://pubman.mpdl.mpg.de/pubman/item/escidoc:995221:8/component/escidoc:995220/MPI_Report354.pdf.]

Rupp, T.S., Chen, Xi, Olson, Mark, and McGuire, A.D., 2007, Sensitivity of simulated boreal fire dynamics to uncertainties in climate drivers: Earth Interactions, v. 11, no. 3, p. 1–21, http://dx.doi.org/10.1175/EI189.1.

Rupp, T.S., Olson, Mark, Adams, L.G., Dale, B.W., Joly, Kyle, Henkleman, Jonathan, Collins, W.B., and Starfield, A.M., 2006, Simulating the influences of various fire regimes on caribou winter habitat: Ecological Applications, v. 16, no. 5, p. 1730–1743, http://dx.doi.org/10.1890/1051-0761(2006)016[1730:STIOVF]2.0.CO;2.

Rupp, T.S., Starfield, A.M., and Chapin, F.S., III, 2000, A frame-based spatially explicit model of subarctic vegetation response to climatic change; Comparison with a point model: Landscape Ecology, v. 15, no. 4, p. 383–400, http://dx.doi.org/10.1023/A:1008168418778.

Rupp, T.S., Starfield, A.M., Chapin, F.S., III, and Duffy, P., 2002, Modeling the impact of black spruce on the fire regime of Alaskan boreal forest: Climatic Change, v. 55, nos. 1–2, p. 213–233, http://dx.doi.org/10.1023/A:1020247405652.

Serreze, M.C., and Francis, J.A., 2006, The Arctic amplification debate: Climatic Change, v. 76, nos. 3–4, p. 241–264, http://dx.doi.org/10.1007/s10584-005-9017-y.

Serreze, M.C., Walsh, J.E., Chapin, F.S., III, Osterkamp, T., Dyurgerov, M., Romanovsky, V., Oechel, W.C., Morison, J., Zhang, T., and Barry, R.G., 2000, Observational evidence of recent change in the northern high-latitude environment: Climatic Change, v. 46, nos. 1–2, p. 159–207, http://dx.doi.org/10.1023/A:1005504031923.

Shulski, Martha, and Wendler, Gerd, 2007, The climate of Alaska: Fairbanks, Alaska, University of Alaska Press, 216 p.

Solomon, Susan, Qin, Dahe, Manning, Martin, Chen, Zhenlin, Marquis, Melinda, Averyt, Kristen, Tignor, M.M.B., and Miller, H.L., Jr., eds., 2007, Climate change 2007—The physical science basis, Contribution of Working Group I to the Fourth Assessment Report of the Intergovernmental Panel on Climate Change: Cambridge, United Kingdom, Cambridge University Press, 996 p. [Also available at https://www.ipcc.ch/publications_and_data/publications_ipcc_fourth_assessment_report_wg1_report_the_physical_science_basis.htm.]

Stafford, J.M., Wendler, G., and Curtis, J., 2000, Temperature and precipitation of Alaska; 50 year trend analysis: Theoretical and Applied Climatology, v. 67, nos. 1–2, p. 33–44, http://dx.doi.org/10.1007/s007040070014.

Strengers, Bart, Leemans, Rik, Eickhout, Bas, de Vries, Bert, and Bouwman, Lex, 2004, The land-use projections and resulting emissions in the IPCC SRES scenarios as simulated by the IMAGE 2.2 model: GeoJournal, v. 61, no. 4, p. 381–393, http://dx.doi.org/10.1007/s10708-004-5054-8.

Turetsky, M.R., Kane, E.S., Harden, J.W., Ottmar, R.D., Manies, K.L., Hoy, Elizabeth, and Kasischke, E.S., 2011, Recent acceleration of biomass burning and carbon losses in Alaskan forests and peatlands: Nature Geoscience, v. 4, no. 1, p. 27–31, http://dx.doi.org/10.1038/ngeo1027.

U.S. Department of Agriculture, National Agricultural Statistics Service, 2014, 2012 census of agriculture; United States summary and State data: U.S. Department of Agriculture, Geographic Area Series, v. 1, pt. 51, 586 p.

Verbyla, David, 2008, The greening and browning of Alaska based on 1982–2003 satellite data: Global Ecology and Biogeography, v. 17, no. 4, p. 547–555, http://dx.doi.org/10.1111/j.1466-8238.2008.00396.x.

Walsh, J.E., Chapman, W.L., Romanovsky, Vladimir, Christensen, J.H., and Stendel, Martin, 2008, Global climate model performance over Alaska and Greenland: Journal of Climate, v. 21, no. 23, p. 6156–6174, http://dx.doi.org/10.1175/2008JCLI2163.1.

Werner, R.A., Holsten, E.H., Matsuoka, S.M., and Burnside, R.E., 2006, Spruce beetles and forest ecosystems in south-central Alaska; A review of 30 years of research: Forest Ecology and Management, v. 227, no. 3, p. 195–206, http://dx.doi.org/10.1016/j.foreco.2006.02.050.

World Meteorological Organization, 2008, Guide to meteorological instruments and methods of observation (7th ed.): Commission for Instruments and Methods of Observation, World Meteorological Organization, no. 8, accessed December 15, 2014, at https://www.wmo.int/pages/prog/www/IMOP/CIMO-Guide.html.

Yoshikawa, Kenji, Bolton, W.R., Romanovsky, V.E., Fukuda, Masami, and Hinzman, L.D., 2002, Impacts of wildfire on the permafrost in the boreal forests of interior Alaska: Journal of Geophysical Research; Atmospheres, v. 107, no. D1, p. FFR 4–1 to FFR 4–14, http://dx.doi.org/10.1029/2001JD000438.